Sinorhizobium meliloti functions required for resistance to antimicrobial NCR peptides and bacteroid differentiation

Quentin Nicoud[1,*], Quentin Barrière[1,*], Nicolas Busset[1,*], Mickaël Bourge[1], Romain Le Bars[1], Claire Boulogne[1], Marie Lecroël[1], Sándor Jenei[2], Atilla Kereszt[2], Eva Kondorosi[2], Tatiana Timtchenko[1], Benoît Alunni[1], Peter Mergaert[1,#]

[1]Université Paris-Saclay, CEA, CNRS, Institute for Integrative Biology of the Cell (I2BC), 91198 Gif-sur-Yvette, France

[2]Institute of Plant Biology, Biological Research Centre, 6726 Szeged, Hungary

*equal contribution

[#]correspondence: peter.mergaert@i2bc.paris-saclay.fr

Running title: NCR resistance in *Sinorhizobium meliloti*

Abstract

Legumes of the *Medicago* genus form symbiosis with the bacterium *Sinorhizobium meliloti* and develop root nodules housing large numbers of the intracellular symbionts. Members of the Nodule-specific Cysteine Rich peptide (NCRs) family induce the endosymbionts into a terminal differentiated state. Individual cationic NCRs are antimicrobial peptides that have the capacity to kill the symbiont but the nodule cell environment prevents killing. Moreover, the bacterial broad-specificity peptide uptake transporter BacA and exopolysaccharides contribute to protect the endosymbionts against the toxic activity of NCRs. Here, we show that other *S. meliloti* functions participate in the protection of the endosymbionts, including an additional broad-specificity peptide uptake transporter encoded by the *yejABEF* genes, lipopolysaccharide modifications mediated by *lpsB* and *lpxXL* as well as *rpoH1*, encoding a stress sigma factor. Mutants in these genes show *in vitro* a strain-specific increased sensitivity profile against a panel of NCRs and form nodules in which bacteroid differentiation is affected. The *lpsB* mutant nodule bacteria do not differentiate, the *lpxXL* and *rpoH1* mutants form some seemingly fully differentiated bacteroids although most of the nodule bacteria are undifferentiated, while the *yejABEF* mutants form hypertrophied but nitrogen-fixing bacteroids. The nodule bacteria of all the mutants have a strongly enhanced membrane permeability, which is dependent on the transport of NCRs to the endosymbionts. Our results suggest that *S. meliloti* relies on a suite of functions including peptide transporters, the bacterial envelope structures and stress response regulators to resist the stressful assault of NCR peptides in the nodule cells.

Importance

The nitrogen fixing symbiosis of legumes with rhizobium bacteria has a predominant ecological role in the nitrogen cycle and has the potential to provide the nitrogen required for plant growth in agriculture. The host plants allow the rhizobia to colonize specific symbiotic organs, the nodules, in large numbers in order to produce sufficient reduced nitrogen for the plant needs. Some legumes, including *Medicago* spp., produce massively antimicrobial peptides to keep this large bacterial population in check. These peptides, known as NCRs, have the potential to kill the rhizobia but in nodules, they only inhibit the division of the bacteria, which maintain a high nitrogen fixing activity. In this study, we show that the tempering of the antimicrobial activity of the NCR peptides in the *Medicago* symbiont *Sinorhizobium meliloti* is multifactorial and requires the YejABEF peptide transporter, the lipopolysaccharide outer membrane and the stress regulator RpoH1.

50 **Introduction**

51 Antimicrobial peptides (AMPs) are a diverse group of defense peptides, which are essential mediators
52 of innate immunity in eukaryotes. Their function is to attack and kill unwanted and potentially harmful
53 invading microbes. Animals deficient in a specific AMP or in the regulation of AMP expression are more
54 sensitive to bacterial or fungal infections, while the ectopic expression of AMPs in animals and plants
55 can enhance resistance (1–3). AMPs are also widely used as essential regulators of bacteria in symbiotic
56 associations (2). In symbiosis, host organisms intentionally maintain bacterial partners and the role of
57 "symbiotic" AMPs is therefore not to eradicate the symbiotic microbes but rather to police them or to
58 optimize their metabolic integration with the hosts (2, 4).

59 An extreme case of deployment of AMPs for controlling endosymbiont populations, involving
60 hundreds of peptides, is described in the rhizobium-legume symbiosis (2, 5–9). Legumes form a
61 symbiosis with phylogenetically diverse nitrogen-fixing soil bacteria, collectively called rhizobia. This
62 nutritional symbiosis provides reduced nitrogen to the plants, enabling them to grow in nitrogen-poor
63 soils that are normally limiting growth. The symbiosis implies the formation of nodules, specific
64 symbiotic organs, on the roots of the plants. These nodules house the nitrogen-fixing rhizobia, which
65 transfer their produced ammonia to the plant in return for the exclusive niche that the plant creates
66 for them in the nodules where they multiply massively from a single or very few infecting bacteria to
67 a population of millions.

68 After endocytic uptake by the symbiotic nodule cells, the multiplied bacteria reside intracellularly in
69 vesicles called symbiosomes. The nodule cells and symbiosomes establish the optimal conditions for
70 nitrogen fixation and metabolic exchange with the endosymbionts and at the same time, keep them
71 in check. The low oxygen levels prevailing in the symbiotic nodule cells transform the rhizobia into a
72 differentiated physiological state, called bacteroid, which is adapted for nitrogen fixation. Moreover,
73 in certain legume clades like the Inverted Repeat Lacking Clade (IRLC) and the Dalbergioids, the
74 physiological transition of the bacteroids is accompanied with a remarkable differentiation process
75 that is manifested in an irreversible loss of the capacity of bacteroids to divide (10, 11). These
76 terminally differentiated bacteroids have a partially permeabilized cell membrane. They are giant
77 bacterial cells, being either long, wide rods, resulting from polar cell elongation, or large spheres,
78 resulting from an isodiametric growth. A switch in the bacterial cell cycle, from a regular cycle of
79 replication and division to a cycle of repeated genome replications without divisions, drives this cell
80 enlargement, resulting in polyploid bacteroids.

81 The terminal differentiation is triggered by a family of Nodule-specific Cysteine-Rich (NCR) peptides,
82 produced by the symbiotic nodule cells (11–13). In *Medicago truncatula*, over 600 *NCR* genes were
83 identified in the genome, and from a few to several hundreds of them are present also in other species
84 of the IRLC and the Dalbergoids (11, 12, 14, 18). The 600 *NCR* genes in *M. truncatula* are specifically

85 expressed in the symbiotic cells (15). However, they are activated in different waves during the
86 differentiation of the symbiotic cells and bacteroids, including sets of *NCR* genes activated at the onset
87 and others at the intermediate or final stages of the differentiation. These temporal profiles indicate
88 that the different *NCR* genes have specific functions during the bacteroid formation process.
89 The NCR peptides have structural features shared with AMPs and at least some NCRs, in particular the
90 cationic ones, can *in vitro* kill or inhibit the growth of not only the rhizobium symbionts but also many
91 other bacteria and even fungi (16). Their major antibacterial activity results from their capacity to
92 disturb the integrity of the inner and outer membranes of bacteria (13, 17), although some NCRs have
93 also inhibiting activities on essential intracellular machineries (18). However, bacteroids remain
94 metabolically active for very long, despite the high burden of NCRs. Possibly, the environment of the
95 symbiotic nodule cells and symbiosomes contribute to temper the antimicrobial activity of the
96 peptides. Importantly, also specific functions of the bacteria themselves are NCR-resistance
97 determinants in the bacteroids.
98 *Sinorhizobium meliloti*, the symbiont of *Medicago* plants, requires the peptide transporter BacA to
99 counter the NCR peptides inside the symbiotic nodule cells and establish a chronic infection (19). *S.*
100 *meliloti bacA* mutants are hypersensitive to the antimicrobial NCRs. They induce nodules and infect
101 their symbiotic cells seemingly normally but the mutants die as soon as they are released in the
102 symbiotic cells. This death can be avoided by blocking NCR transport to the infecting rhizobia in the *M.*
103 *truncatula dnf1* mutant (19). BacA proteins are broad-specificity peptide uptake transporters (20–22).
104 They can promote the uptake of NCR peptides, suggesting that BacA provides resistance by redirecting
105 the peptides away from the bacterial membrane, thereby limiting membrane damage.
106 Exopolysaccharide (EPS) is another known factor of *S. meliloti* that helps the endosymbionts to
107 withstand the NCRs (14, 23). This negatively charged extracellular polysaccharide traps the cationic
108 AMPs, reducing their effective concentration in the membrane vicinity.
109 Bacterial resistance to AMPs is usually multifactorial (24), suggesting that besides BacA and EPS,
110 additional functions of *S. meliloti* bacteroids contribute to resist the NCRs in the symbiotic nodule cells.
111 The literature on *S. meliloti* is rich in the description of bacterial genes that are required for symbiosis.
112 However, often the reporting on these mutants lacks precise information on their bacteroid phenotype
113 and/or on their sensitivity to NCRs. Moreover, transcriptome and Tn-seq (transposon sequencing)
114 analyses of NCR-treated cells and NCR-protein interaction studies identified a whole suite of additional
115 candidate NCR-responsive functions in *S. meliloti* (18, 25–27). Together with BacA and EPS, some of
116 these *S. meliloti* functions may contribute to alleviate the NCR stress on the bacteroids. To test this
117 hypothesis, we have selected in the present study three candidate functions and analyzed the
118 phenotype of the corresponding mutants in NCR resistance and bacteroid formation.

119 **Results**

120 ***Sinorhizobium meliloti* mutants with enhanced sensitivity to NCR peptides**

121 The *S. meliloti* functions selected in this study include a broad specificity peptide uptake transporter
122 encoded by the *yejABEF* genes (SMc02829-SMc02832), lipopolysaccharide (LPS) modifications
123 mediated by *lpsB* (SMc01219) and *lpxXL* (SMc04268) as well as *rpoH1* (SMc00646), encoding a stress
124 sigma factor. The YejABEF ABC transporter was selected on the basis of a genetic screen by Tn-seq in
125 *S. meliloti* revealing that the mutant has an increased sensitivity to the peptide NCR247 (25). LPS
126 structure is one of the major determinants of AMP resistance and sensitivity in Gram-negative bacteria
127 (24, 28). The selected genes *lpsB* and *lpxXL* encode respectively a glycosyltransferase involved in the
128 synthesis of the LPS core and a very-long-chain fatty acid acyl transferase involved in the biosynthesis
129 of lipid A. Mutants in these genes are affected in resistance to AMPs and in symbiosis (29, 30). Finally,
130 the *rpoH1* gene is a global stress regulator in *S. meliloti* (31). The gene as well as its target genes are
131 upregulated in NCR247 treated cells (26, 27). An *rpoH1* mutant is also affected in symbiosis (32). These
132 selected genes are expressed in nodules, with peak expression in different regions of the nodule where
133 bacteria infect plant cells, undergo the differentiation process or fix nitrogen (15, 33)(Fig. S1).
134 Mutants in these candidate genes were constructed (*yejA*, *yejE*, *yejF*, *rpoH1*) or were obtained from
135 previous studies (*lpsB*, *lpxXL*). Log-phase bacteria were treated with a small panel of NCR peptides that
136 were previously shown to have antimicrobial activity (14). These tested peptides were NCR169,
137 NCR183, NCR247 and NCR280, which displayed three different expression patterns in the nodule
138 tissues (15). The *NCR280* gene is expressed in the younger nodule cells, the *NCR169* gene in the older
139 cells while *NCR183* and *NCR247* have an intermediate expression pattern (Fig. S1). The bacterial
140 survival after treatment was determined by counting colony-forming units. The selected mutants were
141 tested along with the wild-type strain and the *bacA* mutant, which was previously shown to be
142 hypersensitive to NCRs (19). The four tested NCR peptides had a strong antimicrobial activity against
143 the wild-type strain, which displayed a survival rate ranging from 8% to 0.03% depending on the tested
144 peptide (Table S1). In agreement with previous results, the *bacA* mutant was hypersensitive to the four
145 peptides (Table S1; Fig. 1). Interestingly, the newly analyzed mutants all displayed a higher sensitivity
146 to at least one of the peptides compared to the wild type (Table S1; Fig. 1). The *lpxXL* mutant was more
147 sensitive to the four peptides, the *lpsB*, *yejE* and *yejF* mutants were more sensitive to NCR183, NCR247
148 and NCR280. The *yejA* mutant was more sensitive to NCR280 and the *rpoH1* mutant was more sensitive
149 to NCR247. The differential response towards peptide NCR247 of the *yejA* mutant on the one hand
150 and the *yejE* and *yejF* mutants on the other hand, corresponds to the previously described Tn-seq
151 screen with this peptide (25). Taken together, this analysis indicated that each mutant displayed a
152 specific sensitivity profile to the panel of tested peptides.

153

154 **Nodule formation by NCR-sensitive *Sinorhizobium meliloti* mutants**

155 Next, the phenotype of these mutants in symbiosis with *M. truncatula* was compared with the wild-
156 type strain and the *bacA* mutant. Measurement of the nitrogen fixation activity and macroscopic
157 inspection of the root system of plants inoculated with the wild type and seven mutants (Fig. S2)
158 revealed that, besides the wild type, mutants in the *yejA*, *yejE*, *yejF* and *lpxXL* genes formed functional
159 nodules (Fix^+), although the *yejE*, *yejF* and *lpxXL* mutants had a reduced nitrogen-fixation activity. On
160 the other hand, the *bacA*, *lpsB* and *rpoH* mutants formed non-functional (Fix^-) and abnormal looking
161 nodules that were small and white, in agreement with previous descriptions (19, 29, 32).

162 The histological organization of the nodules formed by the mutants and the formation of infected
163 symbiotic cells and the viability of the bacteria they contain, were analysed using confocal microscopy
164 (Fig. 2A). The used staining procedure highlights the nodule bacteria with a green fluorescence signal
165 (SYTO^{TM}9) when their membranes are well preserved and with a red fluorescence (propidium iodide)
166 when their membranes are highly permeable. As previously reported, wild-type nodules formed
167 symbiotic cells infected with green-labelled elongated bacteroids, while the nodules infected with the
168 *bacA* mutant contained symbiotic cells carrying small undifferentiated bacteria staining red (19).

169 On the other hand, contrary to what we expected from the macroscopic inspection of the nodules and
170 their ability to fix nitrogen, the *yejA*, *yejE* and *yejF* mutant bacteroids were substantially altered
171 compared to wild-type bacteroids. A high proportion of them were red-stained indicating that their
172 membranes were strongly permeabilized. Nevertheless, other host cells contained bacteroids stained
173 in green by the SYTO^{TM}9 dye. LpxXL is known to be important, but not essential to *S. meliloti* during
174 symbiosis with alfalfa (*Medicago sativa*) (34). The mutant forms hypertrophied bacteroids (30). In our
175 experiments, the *lpxXL* mutant displayed elongated bacteroids but mostly permeable to propidium
176 iodide (stained in red). This observation confirmed that *S. meliloti* LpxXL is also essential for the normal
177 bacteroid differentiation process in *M. truncatula* but that it is not crucial for infection and nitrogen
178 fixation. The *rpoH1* mutant formed elongated bacteroids that were, however, strongly stained by
179 propidium iodide, in agreement with the Fix^- phenotype of the nodules and the described phenotype
180 of the mutant in alfalfa (32). Inside the small bumps elicited by the *lpsB* mutant, no cell seems to be
181 colonised by bacteria as revealed by confocal microscopy. Thus, the *S. meliloti lpsB* mutant failed to
182 colonize the host cells and is defective at an earlier stage in infection than the *bacA* mutant, which
183 does form infected plant cells. It was previously reported that the *lpsB* mutant colonizes nodules cells
184 in *M. sativa* suggesting a more severe defect in *M. truncatula* (35, 36). Therefore, we tested the
185 phenotype of the selected mutants also on *M. sativa* (Fig. S3). The *lpsB*, *rpoH1* and the *yejA* mutants
186 had indeed milder phenotypes on this host while the other mutants had similar phenotypes on the
187 two hosts.

188

189 **Can the increased membrane permeability of the NCR-sensitive *Sinorhizobium meliloti* mutants be**
190 **attributed to the NCRs in nodules?**
191 The high membrane permeability of the nodule bacteria of the *bacA* mutant is the result of the action
192 of the NCR peptides in the nodule cells on this NCR-hypersensitive mutant (19). Possibly, the same is
193 true for the other mutants. To test this hypothesis, we made use of the *M. truncatula dnf1* mutant,
194 which is defective in a nodule-specific subunit of the signal peptidase complex (37). This mutant cannot
195 transport NCR peptides to the symbiosomes (13). As a result, the wild-type *S. meliloti* nodule bacteria
196 in this mutant are not differentiated. The *bacA* mutant, which is strongly permeabilized and stained by
197 propidium iodide in nodules of wild-type *M. truncatula* plants, is not so in the *dnf1* mutant nodule cells
198 because the bacteria are not challenged anymore with the NCRs (Fig. 2B)(19). Similarly to the *bacA*
199 mutant, the *yejA*, *yejE*, *yejF*, *lpxXL* and *rpoH1* mutants did not display membrane permeability, as
200 revealed by the absence of propidium iodide staining, in the infected nodule cells of the *dnf1* mutant
201 (Fig. 2B). This suggests thus that these mutants become membrane-permeabilized by the action of the
202 NCRs and that their symbiotic defects are at least in part due to their hypersensitivity to the NCRs (Fig.
203 1). The *lpsB* mutant did not form detectable nodule-like structures on the *dnf1* roots. We can therefore
204 not conclude on the involvement of the NCR peptides in the symbiotic phenotype of this mutant.
205
206 **Bacteroid differentiation in the NCR-sensitive *Sinorhizobium meliloti***
207 A very strong cell enlargement and an increase in the ploidy level of the bacteria characterize the
208 differentiated bacteroids in *Medicago* nodules. These parameters are readily measured by DAPI
209 staining and flow cytometry (10). The wild-type bacteroids from *M. truncatula* nodules had a high DNA
210 content, over twenty fold higher than the DNA content in free-living *S. meliloti* (Fig. 3) and increased
211 scatter parameters reflecting the cell enlargement (Fig. S4). As previously reported, the nodules
212 infected with the *bacA* mutant did not contain differentiated bacteria (Fig. 3, Fig. S4)(21). The bacteria
213 in nodules induced by the *lpsB* mutant, probably located in infection threads, had a profile that
214 confirmed the complete absence of differentiated bacteria (Fig. 3, Fig. S4). Nodules infected with the
215 *rpoH1* mutant had mostly undifferentiated bacteria although a small amount of fully differentiated
216 cells was detected, as well as cells in an intermediate stage. Also the nodules of the *lpxXL* mutant
217 contained many undifferentiated bacteria as well as fully differentiated ones (Fig. 3, Fig. S4). In
218 contrast, the *yejA*, *yejE* and *yejF* mutant nodules contained large numbers of fully differentiated
219 bacteria (Fig. 3, Fig. S4).
220 It was reported previously that the *lpxXL* mutant formed nodules containing misshapen hypertrophied
221 and larger bacteria than the wild-type bacteroids (30). In our study, this difference was detectable in
222 the flow cytometry measurements showing a higher DAPI fluorescence and scatter for the small
223 portion of differentiated bacteria in these nodules (Fig. 3, Fig. S4). Moreover, we noticed that the

224 bacteroids in the nodules infected with the *yejA*, *yejE* and *yejF* mutants displayed similar higher DNA
225 fluorescence and scatter (Fig. 3, Fig. S4), suggesting that also these bacteroids have abnormal
226 morphologies.
227 These patterns, described here for *M. truncatula* nodules were overall similar in the *M. sativa* host
228 plant although the *rpoH1* mutant showed a higher number of intermediate and fully differentiated
229 bacteroids and the *yejA* mutant had a profile similar to the wild type in nodules at 21 dpi while larger
230 than normal bacteroids were only detected at 32 dpi (Fig. S5). These differences corresponded well
231 with the macroscopic and microscopic differences in the nodules between the two host plants (Fig. 2,
232 Fig. S2, Fig. S3).
233
234 **Defective bacteroid differentiation in *yejE* and *yejF* mutants**
235 To confirm the altered bacteroid morphologies in the *yej* mutants, suggested by the cytometry
236 analysis, the *yejE* and *yejF* mutants were observed at high magnification by microscopy. Confocal and
237 transmission electron microscopy of *M. sativa* nodule sections showed that the nodule cells infected
238 with the *yejE* or *yejF* mutant contained a very heterogeneous population of abnormal bacteroid
239 morphs, including elongated, spherical, pear-shaped or irregular blob-like cells (Fig. 4A, Fig. S6A). These
240 cells contrasted strongly with the narrow, elongated wild-type bacteroids. The difference was also
241 obvious by fluorescence microscopy of preparations of purified nodule bacteria (Fig. 4B). The
242 quantification of cell morphology parameters by image analysis with MicrobeJ of free-living bacteria
243 and the purified nodule bacteria confirmed the irregular forms of *yejE* and *yejF* bacteroids, notably
244 showing that these bacteroids are broader and more spherical than the elongated wild-type bacteroids
245 (Fig. 4C; Fig. S6B). Transmission electron microscopy further showed that the cytoplasm and inner
246 membrane of many of the *yejF* nodule cells was retracted, leaving very large intermembrane spaces,
247 which in some cases even developed into vacuoles, entirely surrounded by cytoplasm. Some cells had
248 multiple vacuoles, small and large (Fig. S6A).
249 The strongly abnormal bacteroids in the *yej* mutants is *a priori* contradictory with the nitrogen fixation
250 activity of these nodules. Expression of the *nifH* gene is a marker for nitrogen-fixing bacteroids (38). A
251 *GFP* gene under the control of the *nifH* promoter was introduced into the wild-type strain and the *bacA*
252 (as a negative control), *yejE* and *yejF* mutants. Analysis of the GFP fluorescence in nodule bacteria of
253 *M. truncatula* (Fig. 5) and *M. sativa* (Fig. S7) by confocal microscopy and flow cytometry showed that
254 despite their aberrant morphology, the *yejE* and *yejF* bacteroids are functional.
255 In contrast to the bacteroids, in the cultured bacteria, no differences were observed in the
256 ultrastructure of the wild-type and *yejF* mutant bacteria (Fig. S8). Moreover, the mutants behaved like
257 wild type in unstressed growth in culture or in the presence of hydrogen peroxide, sodium chloride
258 and acid stress (Fig. S8). On the other hand, the *yej* mutants were more sensitive than wild type to the

259 exposure with the detergent sodium dodecyl sulfate (Fig. S8), indicating that these mutants have a
260 reduced ability to cope with membrane stress. Together, these phenotypes are in agreement with the
261 bacteroid defects resulting from a nodule-specific stress such as one derived from the NCR peptides.
262
263 **NCR247 uptake by the YejABEF transporter**
264 In *E. coli*, both YejABEF and the BacA homolog SbmA mediate the transport of microcin C peptides.
265 Therefore, we tested whether the overlap in substrates of YejABEF and BacA can be extended to NCR
266 peptides which are known substrates of BacA (20, 21). We tested the impact of the mutants in the
267 YejABEF transporter on NCR247 uptake and compared it with a mutation in *bacA*. With a flow
268 cytometry based assay and a fluorescent derivative of the NCR247 peptide, we found that while the
269 NCR247 uptake is completely abolished in the *bacA* mutant, as expected, its uptake is also reduced but
270 not completely abolished in the three *yej* mutants (Fig. 6). This suggests that the YejABEF transporter
271 contributes to NCR uptake.
272
273 **Discussion**
274 **Multiple functions of *Sinorhizobium meliloti* contribute to NCR resistance and are required for**
275 **bacteroid formation and persistence**
276 The NCR peptides are a two-edged sword. On the one hand, they maneuver the rhizobial
277 endosymbionts into a terminally differentiated state via a multitude of activities on the bacteria from
278 which the membrane permeabilization, cell cycle perturbation (polyploidization) and cell enlargement
279 are the most visible ones. On the other hand, NCRs have antimicrobial activity, potentially killing the
280 endosymbionts. Therefore, rhizobia have to defend themselves to be able to establish a chronic
281 infection in the NCR-producing symbiotic cells of the nodules. Previous work has identified the BacA
282 peptide transporter and the EPS barrier in the bacterial envelope as defenses of *Sinorhizobium* strains
283 against the NCRs of their *Medicago* hosts (14, 19, 23).
284 Here, we defined three new functions in *S. meliloti*, the LPS, the sigma factor RpoH1, and the YejABEF
285 peptide transporter as additional determinants in bacteroids, required to cope with the NCR peptides.
286 We show that knockout mutants in these genes are more sensitive to a panel of antimicrobial NCRs
287 and that this hypersensitivity is correlated with a strongly enhanced membrane permeability of the
288 nodule bacteria and abnormalities in their morphology and ploidy levels. It is striking, however, that
289 the different mutants have markedly different bacteroid phenotypes, ranging from undifferentiated
290 to hyper-differentiated. This can be attributed to at least three factors. Each mutant has a specific NCR-
291 sensitivity profile when tested against a small panel of peptides and the "NCR landscape" present in
292 the developing symbiotic cells is continuously changing because of the expression of the hundreds of

293 *NCR* genes in different waves during symbiotic cell differentiation (15). Accordingly, each mutant could
294 accumulate NCR-induced damage at a different rate and reach the breaking point at different stages
295 over the course of the bacteroid differentiation process (Fig. S1). Moreover, the expression pattern of
296 the bacterial genes in the nodule zones is different, suggesting that their principal impact is situated
297 at different stages of the symbiotic cell development and bacteroid differentiation. In addition, we
298 cannot exclude that these genes provide supplementary contributions to the survival of the nodule
299 bacteria, other than the response to the NCR peptides. Nevertheless, blocking the targeting of the NCR
300 peptides to the nodule bacteria by the use of the *M. truncatula dnf1* mutant prevents the membrane
301 permeabilization of the nodule bacteria in the mutants. This observation places the symbiotic role of
302 these bacterial genes downstream of the peptide targeting to the symbiosomes (except for *lpsB*, see
303 below) and links them, at least in part, to the NCRs.
304 The functions of *S. meliloti* described here and before probably picture only part of the full toolkit of
305 this symbiont to survive the NCR challenge. Many additional *S. meliloti* mutants are described with
306 symbiotic phenotypes that are suggestive for a similar contribution to NCR resistance. (26, 39–50). In
307 addition, other genes that could be important for symbiosis, were discovered in a Tn-seq screen with
308 the peptide NCR247 (25). This screen identified here-described functions like the BacA and YejABEF
309 transporters, the LPS and EPS biosynthesis, but also never analyzed functions. It would be of great
310 interest to explore the function of these genes in relation to the NCR response of bacteroids. Note that
311 some of these genes might have escaped identification in previous genetic screens for symbiosis
312 mutants because mutations might provoke only subtle phenotypes with a weak overall effect on
313 nitrogen fixation in standard laboratory conditions but with bacteroid alterations in morphology and
314 persistence as illustrated here with the *yejABEF* mutants.
315
316 **Response to NCR-induced stress regulated by the alternative sigma factor RpoH1**
317 Bacteria deal with different types of stress conditions by global transcriptional responses mediated by
318 alternative sigma factors. As a general classification, the RpoH sigma factors are believed to control
319 cytoplasmic stress responses, while the RpoE sigma factors are known to respond to periplasmic and
320 membrane stress (51). Given the membrane damage provoked by NCRs on the one hand, and the
321 general function in bacteria of RpoE sigma factors in periplasmic and membrane stress response,
322 including in response to AMPs (52), a role of the RpoE regulators of *S. meliloti* in bacteroid
323 differentiation and NCR response could *a priori* have been expected. *S. meliloti* has 11 RpoE-like sigma
324 factors. Remarkably, despite the fact that some RpoEs have a considerable effect on gene
325 transcription, all single mutants, all possible double mutants and even a mutant lacking all 11 genes
326 showed no detectable phenotypic difference with wild type in symbiosis or during many tested free-

327 living growth conditions, including growth in the presence of membrane stresses (53, 54). Thus, the 11
328 *S. meliloti* RpoEs do not have the expected role in regulating the envelope stress response.
329 This role seems to be taken up in part by RpoH in *S. meliloti*, in agreement with its role in symbiosis
330 and NCR resistance and the observation that growth of the *rpoH1* mutant is affected in the presence
331 of various membrane-disrupting agents (32). The latter suggests that RpoH in *S. meliloti* is not
332 respecting the canonical division of labor between alternative sigma factors and that its function is not
333 restricted to cytoplasmic stress but also encompasses membrane stresses. We propose that the here
334 uncovered role of RpoH1 in NCR resistance and in bacteroid differentiation is connected to its
335 regulation of membrane stress.
336
337 **The lipopolysaccharide barrier against NCR membrane damage**
338 In Gram-negative bacteria like rhizobia, LPS constitutes the first point of attack of cationic AMPs. In a
339 two-stage process, AMPs make first electrostatic interactions with the negatively charged LPS, allowing
340 the AMPs to approach the membrane lipids and subsequently to insert into the lipid bilayer, perforate
341 it and translocate into the periplasm (55). The chemical composition of LPS can influence the efficiency
342 of the AMP attack and pathogens have evolved mechanisms to recognize the presence of AMPs and
343 to modify in response the composition of the LPS to lower the potency of the AMP attack (56).
344 *S. meliloti lpsB* encodes a glycosyl transferase that participates in the biosynthesis of the LPS core (57)
345 and the mutation of the gene affects both the core structure and O-antigen polymerization (38, 39).
346 The O-antigen is thought to be a camouflage, masking the membrane and the charges in the
347 membrane vicinity. In the *lpsB* mutant, the shorter O-antigen could be a less efficient shield against
348 the NCRs, offering to the peptides an easier access to membrane-proximal charges resulting in the
349 increased sensitivity of the *lpsB* mutant to the NCRs (this work) as well as to other AMPs (29, 36).
350 The *lpsB* mutant forms nodules on *M. sativa*, which contain infected cells and has a phenotype that is
351 similar to the *bacA* mutant. However, this *lpsB* mutant forms uninfected nodules on *M. truncatula*
352 roots. Therefore, it was not possible to test the implication of NCRs in this symbiotic phenotype with
353 the use of the *dnf1* mutant, since the *DNF1* gene is expressed only in infected nodule cells (37). Since
354 also the *NCR* genes are nearly exclusively expressed in the infected symbiotic cells (15), the blockage
355 of the mutant before release of bacteria into nodule cells suggests that the LPS could provide
356 protection against another stressor produced very early on in the infection process in *M. truncatula*.
357 On the other hand, it was recently reported that some *NCR* genes are expressed in infected root hairs
358 or Nod factor-stimulated root epidermal cells (58, 59). Thus, it is possible that the challenge with these
359 early NCR peptides is already detrimental to the mutant, blocking any further progress in the infection
360 process.

361 LpxXL is a specific acyl transferase that introduces in the lipid A moiety of LPS the very long chain fatty
362 acid 27-OHC28:0 (34). This LpxXL-dependent acylation is expected to make the lipid A hydrophobic,
363 forming the biophysical basis for LpxXL-dependent NCR resistance. Hydrophobic lipid A increases the
364 thickness of the outer layer of the outer membrane and reduces the membrane fluidity, which on its
365 turn prevents or delays AMP insertion and membrane damage. Increasing lipid A hydrophobicity by
366 introducing additional acyl chains is a well-known mechanism used by *Salmonella* to enhance its
367 resistance against host AMPs during infection (56).
368
369 **The YejABEF peptide transporter provides resistance to membrane-damaging peptides and**
370 **sensitizes bacteria to AMPs with intracellular targets**
371 The YejABEF ABC transporter has never been analyzed before in the context of the rhizobium-legume
372 symbiosis. Furthermore, even though this transporter is highly conserved among proteobacteria, its
373 physiological role in whichever bacterium has been characterized only in a few instances. One of them
374 is the uptake of microcin C in *E. coli*. This translation-inhibiting AMP of bacterial origin has no action
375 on the bacterial membrane but has an intracellular target. A mutant in the YejABEF transporter cannot
376 uptake microcin C and is resistant to the AMP (60, 61). Conversely, the *Salmonella* and *Brucella yejABEF*
377 mutants are more sensitive to peptides with membrane-damaging activity such as defensins,
378 polymyxin B, protamine and melittin. Consequently, these mutants have reduced pathogenicity
379 because their capacity to survive in macrophages and in animals is reduced (62, 63). Thus, the
380 increased sensitivity of the *yejA*, *yejE* and *yejF* mutants of *S. meliloti* towards NCRs, which was
381 suggested by Tn-seq (25) and demonstrated here, is coherent with these previous findings.
382 The characteristics of the YejABEF peptide transporter towards membrane-damaging peptides versus
383 peptides with intracellular action are intriguingly parallel to the features of the BacA peptide
384 transporter (SbmA in *E. coli* and *Salmonella*). These latter transporters are required for the import of
385 diverse peptides with intracellular targets (microcins B and J, Bac7, Bac5 and bleomycin) and mutants
386 are therefore resistant to them while the same mutants are hypersensitive to membrane-active
387 peptides (defensins, NCRs) (19, 64, 65). Moreover, the range of peptides that can be imported overlap
388 between these two types of transporters. Both, YejABEF and SbmA can uptake derivatives of microcin
389 C (32). Furthermore, we show that both BacA and YejABEF contribute to NCR247 uptake. Intriguingly,
390 our genetic analysis suggests that both transporters cooperate to import this peptide, since
391 inactivation of one or the other abolishes or strongly reduces uptake. How these two transporters can
392 physically interact and cooperate is an issue of interest for future research. Nevertheless, BacA can
393 function (partially) in the absence of YejABEF while the inverse is not the case. This could be the basis
394 for the markedly different symbiotic phenotype of the *bacA* and *yej* mutants. While the *bacA* mutation
395 is detrimental from the earliest contact with NCRs and bacteria die as soon as they are released from

396 infection threads in the symbiotic cells, the *yej* mutants cope with the NCR peptides much longer and
397 show abnormalities only at the end of the bacteroid differentiation process and bacteroid lifespan. The
398 *yejA* gene encodes the periplasmic binding protein of the transporter. The *yejA* mutant had a different
399 NCR sensitivity profile than the *yejE* and *yejF* mutant and this was correlated with a different symbiotic
400 phenotype in the *M. sativa* host. This suggest that YejA contributes to the interaction of only a subset
401 of the NCR peptides.
402 How does the YejABEF and BacA transporters contribute to resistance to NCRs and other membrane-
403 damaging peptides? The most straightforward model that has been proposed before for BacA (19–21)
404 as well as for the unrelated SapABCDF peptide uptake transporter (66), is the reduction below a critical
405 threshold of the AMP concentration in the vicinity of the inner membrane. Alternatively, the presence
406 or activity of the transporters might indirectly affect the bacterial envelope structure, rendering it
407 more robust against AMPs. The higher sensitivity of the *yej* mutants towards SDS is in agreement with
408 this possibility. A similar detergent sensitivity and membrane alterations were reported in the *bacA*
409 mutant of *S. meliloti* (67).
410
411 **Conclusions**
412 The multifaceted NCR resistance required for symbiosis and chronic infection of the nodule cells
413 mirrors the multitude of AMP resistance mechanisms in animal pathogens, which collectively
414 contribute to the pathogenicity of these bacteria (2, 3, 68). However, one dimension of this strategy in
415 pathogens is not known in *S. meliloti*, and consists of the direct recognition of host AMPs by receptors
416 triggering an adaptive response. Probably the best studied AMP receptor is the two-component
417 regulator PhoPQ in *Salmonella*, which adjusts the LPS composition in response to the presence of host
418 peptides (56). Perhaps the *S. meliloti* ExoS-ChvI or FeuP-FeuQ two component regulators, which are
419 upregulated by NCR treatment and essential for symbiosis (26, 39, 40), form such a regulatory module,
420 recognizing NCRs and controlling an appropriate response in the symbiotic nodule cells. In this respect,
421 it is of interest to note that the rhizobial LPS structure changes strongly in bacteroids of NCR-producing
422 nodules (69, 70).
423 As shown here, rhizobia have to defend themselves to be able to establish a chronic infection in the
424 NCR-producing symbiotic cells of the nodules. On the other hand, the profile of NCR peptides produced
425 in the nodule cells is also determinant for the outcome of the symbiosis and some *M. truncatula*
426 mutants in individual *NCR* genes or *M. truncatula* accessions, expressing specific *NCR* alleles, display
427 incompatibility with *S. meliloti* strains (71–74). Thus, a fine balance must be established in the
428 symbiotic nodule cells between the NCR landscapes and matching multifactorial bacterial
429 countermeasures. Perturbations in the host or in the endosymbiont, as the ones described here,
430 affecting this equilibrium leads to a breakdown of the symbiosis.

431

432 **Materials and Methods**

433 **Bacterial strains, plant growth and nodulation assays and analysis**

434 The procedures for the growth of the *S. meliloti* Sm1021 strain and its derivatives, plant culture of the
435 *M. sativa* cultivar Gabès, the *M. truncatula* accession Jemalong A17, and the A17 *dnf1* mutant,
436 nodulation assays, acetylene reduction assays, bacteroid isolation, flow cytometry measurements and
437 confocal microscopy were performed as described before (75). Bacterial mutants in *rpoH1*, *yejA*, *yejE*
438 and *yejF* were obtained by plasmid insertion and gene deletion (Table S2) as described before (76).
439 Quantitative analysis of the shape of free-living bacteria and bacteroids was performed with the
440 MicrobeJ plugin of ImageJ (77). Bacteroid extracts and exponential phase cultures were stained with
441 2.5 nM SYTO™9 for 10 minutes at 37°C and mounted between slide and coverslip. Bacteria imaging
442 was performed on a SP8 laser scanning confocal microscope (Leica microsystems) equipped with
443 hybrid detectors and a 63x oil immersion objective (Plan Apo, NA: 1.4, Leica). For each condition,
444 multiple z-stacks (2.7µm width, 0.7 µm step) were automatically acquired (excitation: 488 nm;
445 collection of fluorescence: 520-580 nm). Stacks were transformed as maximum intensity projections
446 using ImageJ software (78). Bacteria in the image stacks were automatically detected with MicrobeJ
447 using an intensity based threshold method with a combination of morphological filters. To ensure
448 high data quality every image was manually checked to remove false positive objects (mainly plant
449 residues). Morphological parameters were directly extracted from MicrobeJ and figures were created
450 with Excel or ggplot2 in R.

451

452 ***In vitro* sensitivity and peptide uptake assays**

453 NCR sensitivity assays were carried out essentially as described (20). To measure the resistance of
454 strains to sodium dodecyl sulfate (SDS), H_2O_2, HCl and NaCl stress, overnight cultures of the wild type
455 and mutants were diluted to OD_{600}=0.2. A total of 100 µL of these suspensions was added to 3 ml soft
456 agar (0.7% agar) and poured onto standard 1.5% agar plates. After solidification of the soft agar, filter
457 paper disks (5 mm diameter) were placed on the center of the plate, and 5 µL of 10% (w/v) SDS, 2 M
458 HCl or 30% H_2O_2 was added to the disks. Plates were incubated at 30°C for 3 days, and the diameter of
459 the clearing zone was measured. Peptide uptake assays were performed as described (20, 79).

460

461 **TEM**

462 Bacterial suspensions at OD_{600}=6 or 21 days old nodule samples were incubated in fixative (3%
463 glutaraldehyde, 1% paraformaldehyde in 0.1 M cacodylate, pH 6.8) for one to three hours, and washed
464 with 0.1 M cacodylate buffer, pH 6.8. Samples were then incubated one hour in 1% osmium tetroxide,
465 1.5% potassium ferrocyanide in water. After washing, bacterial suspensions were pelleted in 2% low

466 melting point agarose to facilitate their manipulation. Samples were dehydrated by incubation in
467 increasing concentrations of ethanol (nodule samples for a total of 4 hours in 10-20-30-50-70-90-
468 100%-absolute ethanol-propylene oxide; bacterial pellets for a total of 2 hours in 10-30-50-70-90-
469 100%-absolute ethanol), followed by infiltration with epoxy resin (low viscosity Premix Kit medium,
470 Agar) (for nodule samples, 3 days of infiltration; for bacterial pellets, 24h of infiltration) and
471 polymerization for 24h at 60°C. Ultrathin sections (80-70 nm) were obtained with an ultramicrotome
472 EM UC6 (Leica Microsystems) and collected on formvar carbon-coated copper grids (Agar). Sections
473 were stained with 2% uranyl acetate (Merck) and lead citrate (Agar) before observation with a JEOL
474 JEM-1400 transmission electron microscope operating at 120kV. Images were acquired using a
475 postcolumn high-resolution (11 megapixels) high-speed camera (SC1000 Orius; Gatan) and processed
476 with Digital Micrograph (Gatan).
477
478 **Acknowledgements**
479 We are grateful to Corinne Foucault for assistance with plant experiments and Cynthia Dupas for help
480 with the TEM experiments. QN was supported by a PhD fellowship from the Paris-Saclay University
481 and QB and NB by Post-doc grants from the Agence Nationale de la Recherche. The present work has
482 benefited from Imagerie-Gif core facility supported by the Agence Nationale de la Recherche (ANR-11-
483 EQPX-0029/Morphoscope, ANR-10-INBS-04/FranceBioImaging; ANR-11-IDEX-0003-02/Saclay Plant
484 Sciences). The EK laboratory is supported by the NKFIH Frontline Research project KKP129924 and a
485 Balzan research grant. This work was supported by the LabEx Saclay Plant Sciences-SPS and grants
486 ANR-17-CE20-0011 and ANR-16-CE20-0013 from the Agence Nationale de la Recherche.
487
488 **Author contributions**
489 QN, QB and NB have initiated jointly this work. QN, QB, NB, ML, RL, CB and TT constructed strains and
490 performed nodulation assays. QN, QB, RL, CB and TT performed microscopy and flow cytometry. QB,
491 SJ, AK and EK performed the *in vitro* experiments and provided reagents. QN, QB, NB, TT, BA and PM
492 conceived the study and analyzed the data. PM wrote the manuscript with input from all authors.
493

494 **References**

495 1. Hanson MA, Lemaitre B. 2020. New insights on Drosophila antimicrobial peptide function in host
496 defense and beyond. Curr Opin Immunol 62:22–30.
497 2. Mergaert P. 2018. Role of antimicrobial peptides in controlling symbiotic bacterial populations.
498 Nat Prod Rep 35:336–356.
499 3. Maróti G, Kereszt A, Kondorosi E, Mergaert P. 2011. Natural roles of antimicrobial peptides in
500 microbes, plants and animals. Res Microbiol 162:363–374.
501 4. Mergaert P, Kikuchi Y, Shigenobu S, Nowack ECM. 2017. Metabolic integration of bacterial
502 endosymbionts through antimicrobial peptides. Trends Microbiol 25:703–712.
503 5. Kondorosi E, Mergaert P, Kereszt A. 2013. A paradigm for endosymbiotic life: cell differentiation
504 of *Rhizobium* bacteria provoked by host plant factors. Annu Rev Microbiol 67:611–628.
505 6. Alunni B, Gourion B. 2016. Terminal bacteroid differentiation in the legume-rhizobium symbiosis:
506 nodule-specific cysteine-rich peptides and beyond. New Phytol 211:411–417.
507 7. Pan H, Wang D. 2017. Nodule cysteine-rich peptides maintain a working balance during nitrogen-
508 fixing symbiosis. Nat Plants 3:17048.
509 8. Stonoha-Arther C, Wang D. 2018. Tough love: accommodating intracellular bacteria through
510 directed secretion of antimicrobial peptides during the nitrogen-fixing symbiosis. Curr Opin Plant
511 Biol 44:155–163.
512 9. Roy P, Achom M, Wilkinson H, Lagunas B, Gifford ML. 2020. Symbiotic outcome modified by the
513 diversification from 7 to over 700 nodule-specific cysteine-rich peptides. Genes 11:348.
514 10. Mergaert P, Uchiumi T, Alunni B, Evanno G, Cheron A, Catrice O, Mausset A-E, Barloy-Hubler F,
515 Galibert F, Kondorosi A, Kondorosi E. 2006. Eukaryotic control on bacterial cell cycle and
516 differentiation in the Rhizobium-legume symbiosis. Proc Natl Acad Sci USA 103:5230–5235.
517 11. Czernic P, Gully D, Cartieaux F, Moulin L, Guefrachi I, Patrel D, Pierre O, Fardoux J, Chaintreuil C,
518 Nguyen P, Gressent F, Da Silva C, Poulain J, Wincker P, Rofidal V, Hem S, Barrière Q, Arrighi J-F,
519 Mergaert P, Giraud E. 2015. Convergent evolution of endosymbiont differentiation in Dalbergioid
520 and Inverted Repeat-Lacking Clade legumes mediated by nodule-specific cysteine-rich peptides.
521 Plant Physiol 169:1254–1265.
522 12. Mergaert P, Nikovics K, Kelemen Z, Maunoury N, Vaubert D, Kondorosi A, Kondorosi E. 2003. A
523 novel family in *Medicago truncatula* consisting of more than 300 nodule-specific genes coding
524 for small, secreted polypeptides with conserved cysteine motifs. Plant Physiol 132:161–173.
525 13. Van de Velde W, Zehirov G, Szatmari A, Debreczeny M, Ishihara H, Kevei Z, Farkas A, Mikulass K,
526 Nagy A, Tiricz H, Satiat-Jeunemaître B, Alunni B, Bourge M, Kucho K, Abe M, Kereszt A, Maroti G,
527 Uchiumi T, Kondorosi E, Mergaert P. 2010. Plant peptides govern terminal differentiation of
528 bacteria in symbiosis. Science 327:1122–1126.

529 14. Montiel J, Downie JA, Farkas A, Bihari P, Herczeg R, Bálint B, Mergaert P, Kereszt A, Kondorosi É.
530 2017. Morphotype of bacteroids in different legumes correlates with the number and type of
531 symbiotic NCR peptides. Proc Natl Acad Sci USA 114:5041–5046.
532 15. Guefrachi I, Nagymihaly M, Pislariu CI, Van de Velde W, Ratet P, Mars M, Udvardi MK, Kondorosi
533 E, Mergaert P, Alunni B. 2014. Extreme specificity of *NCR* gene expression in *Medicago*
534 *truncatula*. BMC Genom 15:712.
535 16. Lima RM, Kylarová S, Mergaert P, Kondorosi É. 2020. Unexplored arsenals of legume peptides
536 with potential for their applications in medicine and agriculture. Front Microbiol 11:1307.
537 17. Mikuláss KR, Nagy K, Bogos B, Szegletes Z, Kovács E, Farkas A, Váró G, Kondorosi É, Kereszt A.
538 2016. Antimicrobial nodule-specific cysteine-rich peptides disturb the integrity of bacterial outer
539 and inner membranes and cause loss of membrane potential. Ann Clin Microbiol Antimicrob
540 15:43.
541 18. Farkas A, Maróti G, Durgő H, Györgypál Z, Lima RM, Medzihradszky KF, Kereszt A, Mergaert P,
542 Kondorosi É. 2014. *Medicago truncatula* symbiotic peptide NCR247 contributes to bacteroid
543 differentiation through multiple mechanisms. Proc Natl Acad Sci USA 111:5183–5188.
544 19. Haag AF, Baloban M, Sani M, Kerscher B, Pierre O, Farkas A, Longhi R, Boncompagni E, Hérouart
545 D, Dall'angelo S, Kondorosi E, Zanda M, Mergaert P, Ferguson GP. 2011. Protection of
546 *Sinorhizobium* against host cysteine-rich antimicrobial peptides is critical for symbiosis. PLoS Biol
547 9:e1001169.
548 20. Barrière Q, Guefrachi I, Gully D, Lamouche F, Pierre O, Fardoux J, Chaintreuil C, Alunni B,
549 Timchenko T, Giraud E, Mergaert P. 2017. Integrated roles of BclA and DD-carboxypeptidase 1 in
550 Bradyrhizobium differentiation within NCR-producing and NCR-lacking root nodules. Sci Rep
551 7:9063.
552 21. Guefrachi I, Pierre O, Timchenko T, Alunni B, Barrière Q, Czernic P, Villaécija-Aguilar J-A, Verly C,
553 Bourge M, Fardoux J, Mars M, Kondorosi E, Giraud E, Mergaert P. 2015. *Bradyrhizobium* BclA is a
554 peptide transporter required for bacterial differentiation in symbiosis with *Aeschynomene*
555 legumes. Mol Plant-Microbe Interact 28:1155–1166.
556 22. Rempel S, Gati C, Nijland M, Thangaratnarajah C, Karyolaimos A, de Gier JW, Guskov A, Slotboom
557 DJ. 2020. A mycobacterial ABC transporter mediates the uptake of hydrophilic compounds.
558 Nature 580:409–412.
559 23. Arnold MFF, Penterman J, Shabab M, Chen EJ, Walker GC. 2018. Important late-stage symbiotic
560 role of the *Sinorhizobium meliloti* exopolysaccharide succinoglycan. J Bacteriol 200:e00665-17.
561 24. Cole JN, Nizet V. 2016. Bacterial evasion of host antimicrobial peptide defenses. Microbiol Spectr
562 4.

563 25. Arnold MFF, Shabab M, Penterman J, Boehme KL, Griffitts JS, Walker GC. 2017. Genome-wide
564 sensitivity analysis of the microsymbiont *Sinorhizobium meliloti* to symbiotically important,
565 defensin-like host peptides. mBio 8:e01060-17.
566 26. Penterman J, Abo RP, De Nisco NJ, Arnold MFF, Longhi R, Zanda M, Walker GC. 2014. Host plant
567 peptides elicit a transcriptional response to control the *Sinorhizobium meliloti* cell cycle during
568 symbiosis. Proc Natl Acad Sci USA 111:3561–3566.
569 27. Tiricz H, Szucs A, Farkas A, Pap B, Lima RM, Maróti G, Kondorosi É, Kereszt A. 2013. Antimicrobial
570 nodule-specific cysteine-rich peptides induce membrane depolarization-associated changes in
571 the transcriptome of *Sinorhizobium meliloti*. Appl Environ Microbiol 79:6737–6746.
572 28. Simpson BW, Trent MS. 2019. Pushing the envelope: LPS modifications and their consequences.
573 Nat Rev Microbiol 17:403–416.
574 29. Campbell GRO, Sharypova LA, Scheidle H, Jones KM, Niehaus K, Becker A, Walker GC. 2003.
575 Striking complexity of lipopolysaccharide defects in a collection of *Sinorhizobium meliloti*
576 mutants. J Bacteriol 185:3853–3862.
577 30. Haag AF, Wehmeier S, Beck S, Marlow VL, Fletcher V, James EK, Ferguson GP. 2009. The
578 *Sinorhizobium meliloti* LpxXL and AcpXL proteins play important roles in bacteroid development
579 within alfalfa. J Bacteriol 191:4681–4686.
580 31. Barnett MJ, Bittner AN, Toman CJ, Oke V, Long SR. 2012. Dual RpoH sigma factors and
581 transcriptional plasticity in a symbiotic bacterium. J Bacteriol 194:4983–4994.
582 32. Mitsui H, Sato T, Sato Y, Ito N, Minamisawa K. 2004. *Sinorhizobium meliloti* RpoH1 is required for
583 effective nitrogen-fixing symbiosis with alfalfa. Mol Genet Genom 271:416–425.
584 33. Roux B, Rodde N, Jardinaud M-F, Timmers T, Sauviac L, Cottret L, Carrère S, Sallet E, Courcelle E,
585 Moreau S, Debellé F, Capela D, de Carvalho-Niebel F, Gouzy J, Bruand C, Gamas P. 2014. An
586 integrated analysis of plant and bacterial gene expression in symbiotic root nodules using laser-
587 capture microdissection coupled to RNA sequencing. Plant J 77:817–837.
588 34. Ferguson GP, Datta A, Carlson RW, Walker GC. 2005. Importance of unusually modified lipid A in
589 *Sinorhizobium* stress resistance and legume symbiosis. Mol Microbiol 56:68–80.
590 35. Niehaus K, Lagares A, Pühler A. 1998. A *Sinorhizobium meliloti* lipopolysaccharide mutant
591 induces effective nodules on the host plant *Medicago sativa* (alfalfa) but fails to establish a
592 symbiosis with *Medicago truncatula*. Mol Plant-Microbe Interact 11:906–914.
593 36. Campbell GRO, Reuhs BL, Walker GC. 2002. Chronic intracellular infection of alfalfa nodules by
594 *Sinorhizobium meliloti* requires correct lipopolysaccharide core. Proc Natl Acad Sci USA 99:3938–
595 3943.

596 37. Wang D, Griffitts J, Starker C, Fedorova E, Limpens E, Ivanov S, Bisseling T, Long S. 2010. A
597 nodule-specific protein secretory pathway required for nitrogen-fixing symbiosis. Science
598 327:1126–1129.
599 38. Mendoza-Suárez MA, Geddes BA, Sánchez-Cañizares C, Ramírez-González RH, Kirchhelle C, Jorrin
600 B, Poole PS. 2020. Optimizing *Rhizobium*-legume symbioses by simultaneous measurement of
601 rhizobial competitiveness and N_2 fixation in nodules. Proc Natl Acad Sci USA 117:9822–9831.
602 39. Bélanger L, Dimmick KA, Fleming JS, Charles TC. 2009. Null mutations in *Sinorhizobium meliloti*
603 *exoS* and *chvI* demonstrate the importance of this two-component regulatory system for
604 symbiosis. Mol Microbiol 74:1223–1237.
605 40. Griffitts JS, Carlyon RE, Erickson JH, Moulton JL, Barnett MJ, Toman CJ, Long SR. 2008. A
606 *Sinorhizobium meliloti* osmosensory two-component system required for cyclic glucan export
607 and symbiosis. Mol Microbiol 69:479–490.
608 41. Santos R, Hérouart D, Puppo A, Touati D. 2000. Critical protective role of bacterial superoxide
609 dismutase in rhizobium-legume symbiosis. Mol Microbiol 38:750–759.
610 42. Jamet A, Sigaud S, Van de Sype G, Puppo A, Hérouart D. 2003. Expression of the bacterial
611 catalase genes during *Sinorhizobium meliloti-Medicago sativa* symbiosis and their crucial role
612 during the infection process. Mol Plant-Microbe Interact 16:217–225.
613 43. Castro-Sowinski S, Matan O, Bonafede P, Okon Y. 2007. A thioredoxin of *Sinorhizobium meliloti*
614 CE52G is required for melanin production and symbiotic nitrogen fixation. Mol Plant-Microbe
615 Interact 20:986–993.
616 44. Benyamina SM, Baldacci-Cresp F, Couturier J, Chibani K, Hopkins J, Bekki A, de Lajudie P, Rouhier
617 N, Jacquot J-P, Alloing G, Puppo A, Frendo P. 2013. Two Sinorhizobium meliloti glutaredoxins
618 regulate iron metabolism and symbiotic bacteroid differentiation. Environ Microbiol 15:795–810.
619 45. Tang G, Li N, Liu Y, Yu L, Yan J, Luo L. 2018. *Sinorhizobium meliloti* glutathione reductase is
620 required for both redox homeostasis and symbiosis. Appl Environ Microbiol 84:e01937-17.
621 46. Yang L, El Msehli S, Benyamina S, Lambert A, Hopkins J, Cazareth J, Pierre O, Hérouart D, Achi-
622 Smiti S, Boncompagni E, Frendo P. 2020. Glutathione deficiency in *Sinorhizobium meliloti* does
623 not impair bacteroid differentiation but induces early senescence in the interaction with
624 *Medicago truncatula*. Front Plant Sci 11:137.
625 47. Tang G, Xing S, Wang S, Yu L, Li X, Staehelin C, Yang M, Luo L. 2017. Regulation of cysteine
626 residues in LsrB proteins from *Sinorhizobium meliloti* under free-living and symbiotic oxidative
627 stress. Environ Microbiol 19:5130–5145.
628 48. Bittner AN, Foltz A, Oke V. 2007. Only one of five *groEL* genes is required for viability and
629 successful symbiosis in *Sinorhizobium meliloti*. J Bacteriol 189:1884–1889.

630 49. Ogden AJ, McAleer JM, Kahn ML. 2019. Characterization of the *Sinorhizobium meliloti* HslUV and
631 ClpXP protease systems in free-living and symbiotic states. J Bacteriol 201:e00498-18.
632 50. Cosme AM, Becker A, Santos MR, Sharypova LA, Santos PM, Moreira LM. 2008. The outer
633 membrane protein TolC from *Sinorhizobium meliloti* affects protein secretion, polysaccharide
634 biosynthesis, antimicrobial resistance, and symbiosis. Mol Plant-Microbe Interact 21:947–957.
635 51. Gruber TM, Gross CA. 2003. Multiple sigma subunits and the partitioning of bacterial
636 transcription space. Annu Rev Microbiol 57:441–466.
637 52. Guest RL, Raivio TL. 2016. Role of the gram-negative envelope stress response in the presence of
638 antimicrobial agents. Trends Microbiol 24:377–390.
639 53. Sauviac L, Philippe H, Phok K, Bruand C. 2007. An extracytoplasmic function sigma factor acts as a
640 general stress response regulator in *Sinorhizobium meliloti*. J Bacteriol 189:4204–4216.
641 54. Lang C, Barnett MJ, Fisher RF, Smith LS, Diodati ME, Long SR. 2018. Most S*inorhizobium meliloti*
642 extracytoplasmic function sigma factors control accessory functions. mSphere 3:e00454-18.
643 55. Zasloff M. 2002. Antimicrobial peptides of multicellular organisms. Nature 415:389–395.
644 56. Dalebroux ZD, Miller SI. 2014. *Salmonellae* PhoPQ regulation of the outer membrane to resist
645 innate immunity. Curr Opin Microbiol 17:106–113.
646 57. Lagares A, Hozbor DF, Niehaus K, Otero AJ, Lorenzen J, Arnold W, Pühler A. 2001. Genetic
647 characterization of a Sinorhizobium meliloti chromosomal region in lipopolysaccharide
648 biosynthesis. J Bacteriol 183:1248–1258.
649 58. Jardinaud M-F, Boivin S, Rodde N, Catrice O, Kisiala A, Lepage A, Moreau S, Roux B, Cottret L,
650 Sallet E, Brault M, Emery RJN, Gouzy J, Frugier F, Gamas P. 2016. A laser dissection-RNAseq
651 analysis highlights the activation of cytokinin pathways by Nod factors in the *Medicago*
652 *truncatula* root epidermis. Plant Physiol 171:2256–2276.
653 59. Liu C-W, Breakspear A, Guan D, Cerri MR, Jackson K, Jiang S, Robson F, Radhakrishnan GV, Roy S,
654 Bone C, Stacey N, Rogers C, Trick M, Niebel A, Oldroyd GED, de Carvalho-Niebel F, Murray JD.
655 2019. NIN Acts as a network hub controlling a growth module required for rhizobial infection.
656 Plant Physiol 179:1704–1722.
657 60. Bantysh O, Serebryakova M, Zukher I, Kulikovsky A, Tsibulskaya D, Dubiley S, Severinov K. 2015.
658 Enzymatic synthesis and functional characterization of bioactive Microcin C-like compounds with
659 altered peptide sequence and length. J Bacteriol 197:3133–3141.
660 61. Novikova M, Metlitskaya A, Datsenko K, Kazakov T, Kazakov A, Wanner B, Severinov K. 2007. The
661 *Escherichia coli* Yej transporter is required for the uptake of translation inhibitor microcin C. J
662 Bacteriol 189:8361–8365.

663 62. Eswarappa SM, Panguluri KK, Hensel M, Chakravortty D. 2008. The yejABEF operon of Salmonella
664 confers resistance to antimicrobial peptides and contributes to its virulence. Microbiology
665 154:666–678.
666 63. Wang Z, Bie P, Cheng J, Lu L, Cui B, Wu Q. 2016. The ABC transporter YejABEF is required for
667 resistance to antimicrobial peptides and the virulence of *Brucella melitensis*. Sci Rep 6:31876.
668 64. Wehmeier S, Arnold MFF, Marlow VL, Aouida M, Myka KK, Fletcher V, Benincasa M, Scocchi M,
669 Ramotar D, Ferguson GP. 2010. Internalization of a thiazole-modified peptide in *Sinorhizobium*
670 *meliloti* occurs by BacA-dependent and -independent mechanisms. Microbiology 156:2702–
671 2713.
672 65. Arnold MFF, Haag AF, Capewell S, Boshoff HI, James EK, McDonald R, Mair I, Mitchell AM,
673 Kerscher B, Mitchell TJ, Mergaert P, Barry CE, Scocchi M, Zanda M, Campopiano DJ, Ferguson GP.
674 2013. Partial complementation of *Sinorhizobium meliloti bacA* mutant phenotypes by the
675 *Mycobacterium tuberculosis* BacA protein. J Bacteriol 195:389–398.
676 66. Parra-Lopez C, Baer MT, Groisman EA. 1993. Molecular genetic analysis of a locus required for
677 resistance to antimicrobial peptides in *Salmonella typhimurium*. EMBO J 12:4053–4062.
678 67. Ferguson GP, Roop RM, Walker GC. 2002. Deficiency of a *Sinorhizobium meliloti* BacA mutant in
679 alfalfa symbiosis correlates with alteration of the cell envelope. J Bacteriol 184:5625–5632.
680 68. Bauer ME, Shafer WM. 2015. On the *in vivo* significance of bacterial resistance to antimicrobial
681 peptides. Biochim Biophys Acta 1848:3101–3111.
682 69. Kannenberg EL, Carlson RW. 2001. Lipid A and O-chain modifications cause *Rhizobium*
683 lipopolysaccharides to become hydrophobic during bacteroid development. Mol Microbiol
684 39:379–391.
685 70. Crespo-Rivas JC, Guefrachi I, Mok KC, Villaécija-Aguilar JA, Acosta-Jurado S, Pierre O, Ruiz-Sainz
686 JE, Taga ME, Mergaert P, Vinardell JM. 2016. *Sinorhizobium fredii* HH103 bacteroids are not
687 terminally differentiated and show altered O-antigen in nodules of the Inverted Repeat-Lacking
688 Clade legume *Glycyrrhiza uralensis*. Environ Microbiol 18:2392–2404.
689 71. Kim M, Chen Y, Xi J, Waters C, Chen R, Wang D. 2015. An antimicrobial peptide essential for
690 bacterial survival in the nitrogen-fixing symbiosis. Proc Natl Acad Sci USA 112:15238–15243.
691 72. Horváth B, Domonkos Á, Kereszt A, Szűcs A, Ábrahám E, Ayaydin F, Bóka K, Chen Y, Chen R,
692 Murray JD, Udvardi MK, Kondorosi É, Kaló P. 2015. Loss of the nodule-specific cysteine rich
693 peptide, NCR169, abolishes symbiotic nitrogen fixation in the *Medicago truncatula dnf7* mutant.
694 Proc Natl Acad Sci USA 112:15232–15237.
695 73. Wang Q, Yang S, Liu J, Terecskei K, Ábrahám E, Gombár A, Domonkos Á, Szűcs A, Körmöczi P,
696 Wang T, Fodor L, Mao L, Fei Z, Kondorosi É, Kaló P, Kereszt A, Zhu H. 2017. Host-secreted

697 antimicrobial peptide enforces symbiotic selectivity in *Medicago truncatula*. Proc Natl Acad Sci
698 USA 114:6854–6859.
699 74. Yang S, Wang Q, Fedorova E, Liu J, Qin Q, Zheng Q, Price PA, Pan H, Wang D, Griffitts JS, Bisseling
700 T, Zhu H. 2017. Microsymbiont discrimination mediated by a host-secreted peptide in *Medicago*
701 *truncatula*. Proc Natl Acad Sci USA 114:6848–6853.
702 75. Kazmierczak T, Nagymihály M, Lamouche F, Barrière Q, Guefrachi I, Alunni B, Ouadghiri M,
703 Ibijbijen J, Kondorosi É, Mergaert P, Gruber V. 2017. Specific host-responsive associations
704 between *Medicago truncatula* accessions and *Sinorhizobium* strains. Mol Plant-Microbe Interact
705 30:399–409.
706 76. Gully D, Gargani D, Bonaldi K, Grangeteau C, Chaintreuil C, Fardoux J, Nguyen P, Marchetti R,
707 Nouwen N, Molinaro A, Mergaert P, Giraud E. 2016. A peptidoglycan-remodeling enzyme is
708 critical for bacteroid differentiation in *Bradyrhizobium* spp. during legume symbiosis. Mol Plant-
709 Microbe Interact 29:447–457.
710 77. Ducret A, Quardokus EM, Brun YV. 2016. MicrobeJ, a tool for high throughput bacterial cell
711 detection and quantitative analysis. Nat Microbiol 1:16077.
712 78. Schneider CA, Rasband WS, Eliceiri KW. 2012. NIH Image to ImageJ: 25 years of image analysis.
713 Nat Methods 9:671–675.
714 79. Benincasa M, Barrière Q, Runti G, Pierre O, Bourge M, Scocchi M, Mergaert P. 2016. Single Cell
715 Flow Cytometry Assay for Peptide Uptake by Bacteria. Bio-protocol 6:e2038–e2038.
716

717 **Figure legends**

718

719 **Figure 1. Sensitivity profile of *Sinorhizobium meliloti* strains to a panel of NCR peptides.** The heatmap
720 shows the relative survival, expressed in % of the mutant strains compared to the wild type (WT)
721 survival set at 100% for each peptide treatment.

722

723 **Figure 2. Symbiotic phenotype of *Sinorhizobium meliloti* Sm1021 mutants during symbiosis with**
724 ***Medicago truncatula* wild type and *dnf1* mutant. A.** Membrane permeability in bacteroids of *S.*
725 *meliloti* Sm1021 wild type (WT) and mutants in wild-type *M. truncatula* nodules, determined by live-
726 dead staining of nodule sections and confocal microscopy. **B.** Membrane permeability of *S. meliloti*
727 Sm1021 WT and mutants in nodules of the *M. truncatula dnf1* mutant, determined by live-dead
728 staining of nodule sections and confocal microscopy. Nodule phenotype at 21 days post inoculation.
729 Top row images, full nodule sections; Bottom row images, enlarged images of symbiotic cells. Scale
730 bars are indicated in each panel. The staining procedure of nodule sections with a mixture of the dyes
731 propidium iodide, SYTO™9 and calcofluor-white highlights the bacteroids and nodule bacteria with a
732 green fluorescence signal (SYTO™9) when their membranes are well preserved and with a red
733 fluorescence (propidium iodide) when their membranes are highly permeable. Plant cell walls are
734 stained blue (calcofluor-white).

735

736 **Figure 3. DNA content of nodule bacteria in *Medicago truncatula*.** Flow cytometry analysis of the DNA
737 content of bacteria in culture or isolated from nodules infected with the indicated strains and stained
738 with 4',6-diamidino-2-phenylindole (DAPI). The cell counts (y-axes) are represented in function of the
739 DAPI fluorescence intensity (x-axes). The arrow in each graph indicates the mean DNA content of wild-
740 type (WT) bacteroids as in the upper left panel.

741

742 **Figure 4. Bacteroid morphology of *yejE* and *yejF* mutants in *Medicago sativa* nodules. A.** Sections of
743 nodules infected with the wild type (WT) and the *yejE* or *yejF* mutants were stained with a mixture of
744 the dyes propidium iodide, SYTO™9 and calcofluor-white and observed by confocal microscopy. Scale
745 bars (10 µm) are indicated in each panel. **B.** Preparations of cultured bacteria or purified *M. sativa*
746 nodule bacteria of the wild type and the *yejF* mutant were observed by fluorescence microscopy. The
747 panels are composite images and the shown individual cells were cut from original images and
748 recombined in a single panel. Each panel is at the same magnification and the scale bar (10 µm) is
749 indicated in the left panel. **C.** Cell shape parameters of free-living bacteria and bacteroids determined
750 by MicrobeJ. Dot plots show the mean width and length of cells of the indicated strains. Each point
751 represents the values of one bacterium. Numbers of analysed cells (n) are indicated.

752

753 **Figure 5. Nitrogenase expression in the *yejE* and *yejF* mutant bacteroids in *Medicago truncatula***
754 **nodules. A.** Confocal microscopy of sections of nodules infected with *S. meliloti* Sm1021.p*pnifH-GFP*
755 (WT), *bacA*.p*pnifH-GFP* (*bacA*), *yejE*.p*pnifH-GFP* (*yejE*) or *yejF*.p*pnifH-GFP* (*yejF*) and stained with
756 propidium iodide. **B.** Flow cytometry of GFP levels in differentiated nodule bacteria (upper panels) and
757 heat-killed nodule bacteria (lower panels). The green square shows the position of the GFP-positive
758 bacteroids.

759

760 **Figure 6. Uptake of NCR247 mediated by YejABEF.** Flow cytometry assay of the NCR247-FITC peptide.
761 In the WT, a subpopulation of the bacteria import the NCR247-FITC peptide and in the *bacA* mutant,
762 this population is absent. In the *yejA*, *yejE* and *yejF* mutants, the FITC-positive subpopulation is strongly
763 reduced compared to wild type.

764

765 **Figure S1. Expression pattern in nodules of bacterial and *NCR* genes. A.** Schematic drawing of a
766 *Medicago* nodule organized in tissues. The meristem is bacteria-free and contains dividing cells
767 allowing the organ to grow. In the early infection zone, bacteria proliferate in infection threads (green
768 lines) and are released by endocytosis inside cells derived from the meristem. In the late infection zone
769 and the so-called interzone, the bacteria differentiate into bacteroids. The fixation zone contains the
770 fully differentiated, nitrogen-fixing bacteroids. The pictures show bacteria inside the nodule cells and
771 are presented at the same scale (bar is 1 µm) allowing to appreciate the transformation of the bacteria.
772 **B.** Against the backdrop of a changing landscape of NCR peptides (rainbow colors representing
773 peptides appearing and disappearing at different stages of symbiotic cell differentiation), the bacterial
774 functions described in this study are critical at distinct stages of the bacteroid differentiation process.
775 It should be noted that the functions that are essential in early stages, such as LpsB and BacA, can also
776 be important in later stages of the bacteroid differentiation. However, the phenotypic analysis of the
777 corresponding mutants cannot reveal these putative late roles. **C,D.** The relative expression profile (%
778 of total) of the studied bacterial genes *lpsB*, *lpxXL*, *rpoH1*, *yejF*, *yejE*, *yejB*, *yejA* and *bacA* (**C**) and of
779 *NCR280*, *NCR247*, *NCR183* and *NCR169* (**D**) in the meristem, early infection zone, late infection zone,
780 interzone and fixation zone are displayed. Data was extracted from (15) and was obtained by RNA-seq
781 analysis on laser-microdissected nodule tissues (33).

782

783 **Figure S2. Symbiotic phenotypes of NCR sensitivity mutants in *Medicago truncatula*. A.** Nitrogen
784 fixation activity determined by the acetylene reduction assay on whole roots of nodulated plants
785 infected with the indicated bacterial mutants at 21 days post inoculation. NI, non-inoculated control
786 plants; WT, plants nodulated by the wild-type strain Sm1021. Boxplots were generated from 15 plants

787 each. Letters associated with each condition represent statistically different classes determined by a
788 non-parametric Dunn test, with a α threshold equal to 0.05. **B.** Nodule phenotypes at 21 days post
789 inoculation. Arrowheads indicate small nodules elicited by the *lpsB* mutant. Scale bar (2 mm) applies
790 to all panels.
791
792 **Figure S3. Symbiotic phenotype of *Sinorhizobium meliloti* Sm1021 mutants during symbiosis with**
793 ***Medicago sativa*. A.** Leaves of plants inoculated with the indicated strains. Scale bar = 2 cm. **B.** Nodule
794 phenotype at 21 days post inoculation. Scale bar = 1 mm. **C.** Bacteroid viability determined by live-
795 dead staining of nodule sections and confocal microscopy. Top row images, full nodule sections;
796 Bottom row images, enlarged images of symbiotic cells. Scale bars are indicated in each panel. **D.**
797 Composite image of a *yejF*-infected nodule section showing the rapid permeabilization of the
798 membranes of the internalized bacteria (red staining). Note the bacteria in infection threads (white
799 arrows) are not permeabilized (green staining). The images of the composition are separated by
800 dashed lines. **E.** Nitrogen fixation activity determined by the acetylene reduction assay on whole roots
801 of nodulated plants infected with the indicated bacterial mutants at 21 days post inoculation. NI, non-
802 inoculated control plants; WT, plants nodulated by the wild-type strain Sm1021. Boxplots were
803 generated from 15 plants each. Letters associated with each condition represent statistically different
804 classes determined by a non-parametric Dunn test, with a α threshold equal to 0.05.
805
806 **Figure S4. Morphological parameters in nodule bacteria of *Medicago truncatula* nodules.** Flow
807 cytometry analysis of the morphology of bacteria isolated from nodules infected with the indicated
808 strains. The forward scatter (FSC, y-axes) is represented in function of the side scatter (SSC, x-axes).
809 The "X" indicates the peak values for each sample. The position of the peak value in the cultured
810 bacteria and in the wild-type bacteroids are indicated in each panel by the hatched lines.
811
812 **Figure S5. DNA content and morphological parameters in nodule bacteria in *Medicago sativa*. A.**
813 Flow cytometry analysis of the DNA content of bacteria in culture or isolated from nodules infected
814 with the indicated strains and stained with 4',6-diamidino-2-phenylindole (DAPI). The cell counts (y-
815 axes) are represented in function of the DAPI fluorescence (x-axes). The arrow indicates the mean DNA
816 content of wild-type bacteroids. The rows represent three sets of independent experiments and the
817 values of DAPI fluorescence cannot be compared between experiments because of differences in
818 instrument settings. The first two rows are samples prepared from 21 dpi nodules; the third row is
819 from 32 dpi nodules. The latter shows that the phenotype of the *yejA* mutant evolves in older nodules.
820 **B.** Flow cytometry analysis of the morphology of bacteria isolated from nodules infected with the

821 indicated strains. The forward scatter (FSC, y-axes) is represented in function of the side scatter (SSC,
822 x-axes).
823
824 **Figure S6. Cellular defects in the *yejF* mutant bacteroids in *Medicago sativa* nodules. A.** Transmission
825 electron microscopy of wild-type and *yejF* mutant bacteroids. The arrows indicate retracted
826 innermbranes in the yejF bacteroids, "v" indicate vacuoles, "a" indicate amyloplasts and "*" indicate
827 an enlarged peribacteroid space found in the angle of a branched bacteroid. **B.** Boxplots of morphology
828 parameters of free-living bacteria and bacteroids of the indicated strains, measured by MicrobeJ. Area
829 is the measure of the surface; circularity is calculated by $4\pi * area / \text{perimeter}^2$, and describes how close
830 an object is to a perfect circle (value of 1); aspectRatio is the ratio of small and large diameters of the
831 objects' fitted ellipses; width.stdev is the standard deviation calculated from all the measured widths
832 along an object's medial axis. On each graph, panels group measurements made on one strain, either
833 in culture (left box) or extracted from mature nodules (right box). Numbers of analysed cells (n) are
834 identical as in Fig. 4C.
835
836 **Figure S7. Nitrogenase expression in the *yejE* and *yejF* mutant bacteroids in *Medicago sativa***
837 **nodules. A.** Confocal microscopy of sections of nodules infected with *S. meliloti* Sm1021.p*pnifH-GFP*,
838 *bacA*.p*pnifH-GFP*, *yejE*.p*pnifH-GFP* or *yejF*.p*pnifH-GFP* and stained with propidium iodide. **B.** Flow
839 cytometry of GFP levels in differentiated nodule bacteria (upper panels) and heat killed nodule bacteria
840 (lower panels). The square shows the position of the GFP-positive bacteroids.
841
842 **Figure S8. Phenotypes of wild-type and *yej* mutant bacteria in culture. A.** Ultrastructure by
843 transmission electron microscopy. Scale bars are 1 µm. **B.** Growth in liquid medium. **C.** Growth
844 inhibition in the presence of SDS. **D.** Growth inhibition in the presence of H_2O_2. **E.** Growth inhibition in
845 the presence of HCl. **F.** Growth inhibition in the presence of NaCl. Growth inhibitions in C. to F. were
846 determined by the size of a halo formed around a round paper patch soaked in the stress compound.
847
848 **Table S1. Survival after NCR treatment of wild-type and mutant *Sinorhizobium meliloti*.**
849
850 **Table S2. Primers used for mutant construction.**

Figure 1

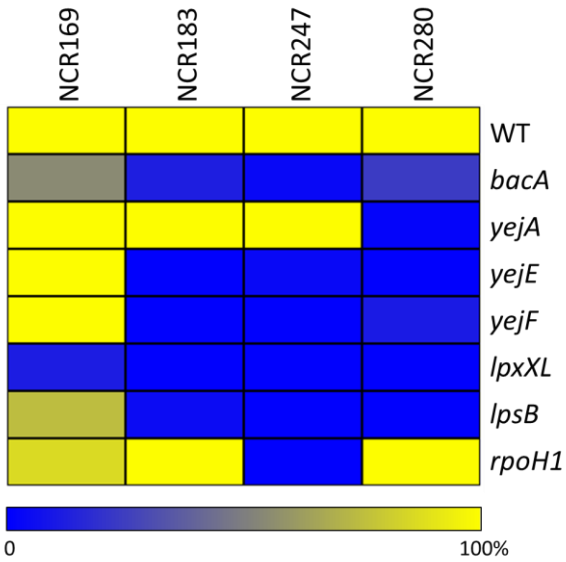
NCR169
NCR183
NCR247
NCR280
WT
bacA
yejA
yejE
yejF
lpxXL
lpsB
rpoH1
0
100%

Figure 2

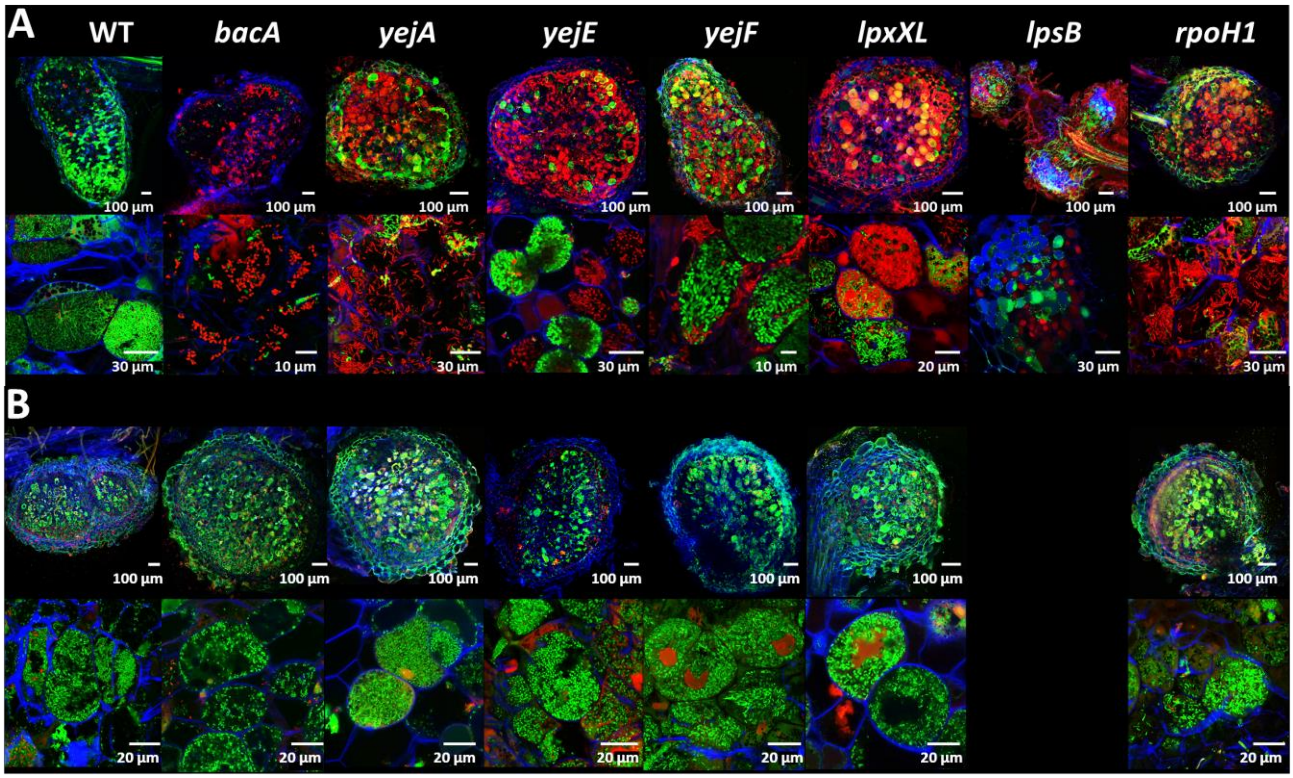
A
WT
bacA
yejA
yejE
yejF
lpxXL
lpsB
rpoH1
100 µm
30 µm
10 µm
20 µm
B

Figure 3

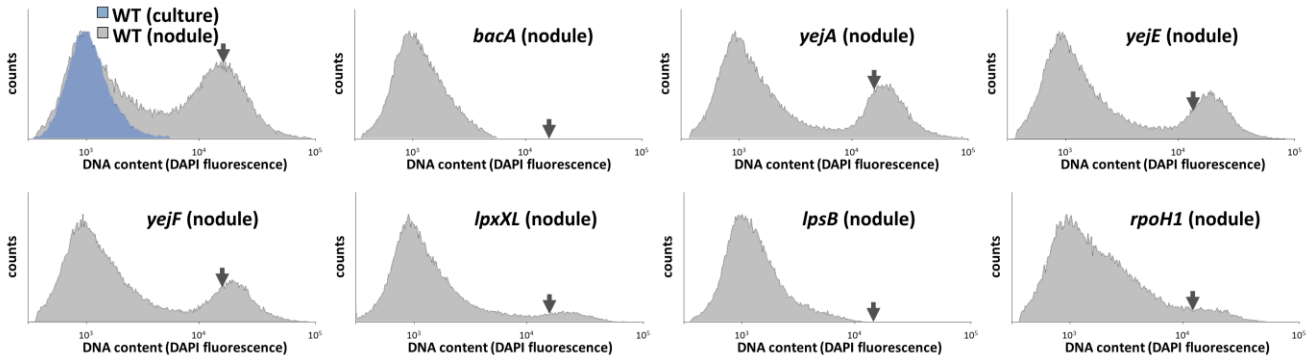
WT (culture)
WT (nodule)
counts
DNA content (DAPI fluorescence)
bacA (nodule)
yejA (nodule)
yejE (nodule)
yejF (nodule)
lpxXL (nodule)
lpsB (nodule)
rpoH1 (nodule)

Figure 4

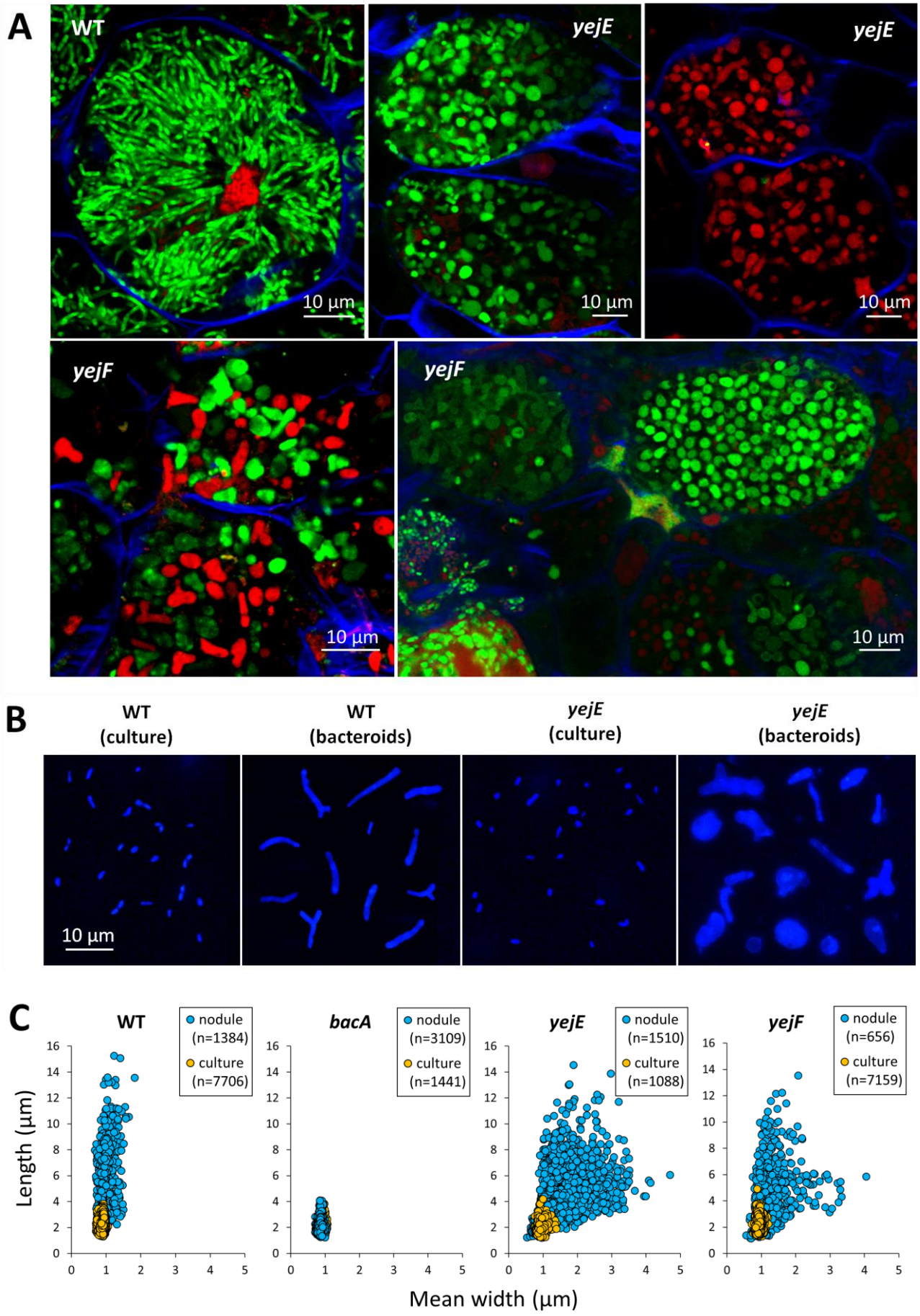
A
WT
yejE
yejE
yejF
yejF
10 µm
B
WT (culture)
WT (bacteroids)
yejE (culture)
yejE (bacteroids)
10 µm
C
WT
bacA
yejE
yejF
nodule (n=1384)
culture (n=7706)
nodule (n=3109)
culture (n=1441)
nodule (n=1510)
culture (n=1088)
nodule (n=656)
culture (n=7159)
Length (µm)
Mean width (µm)

Figure 5

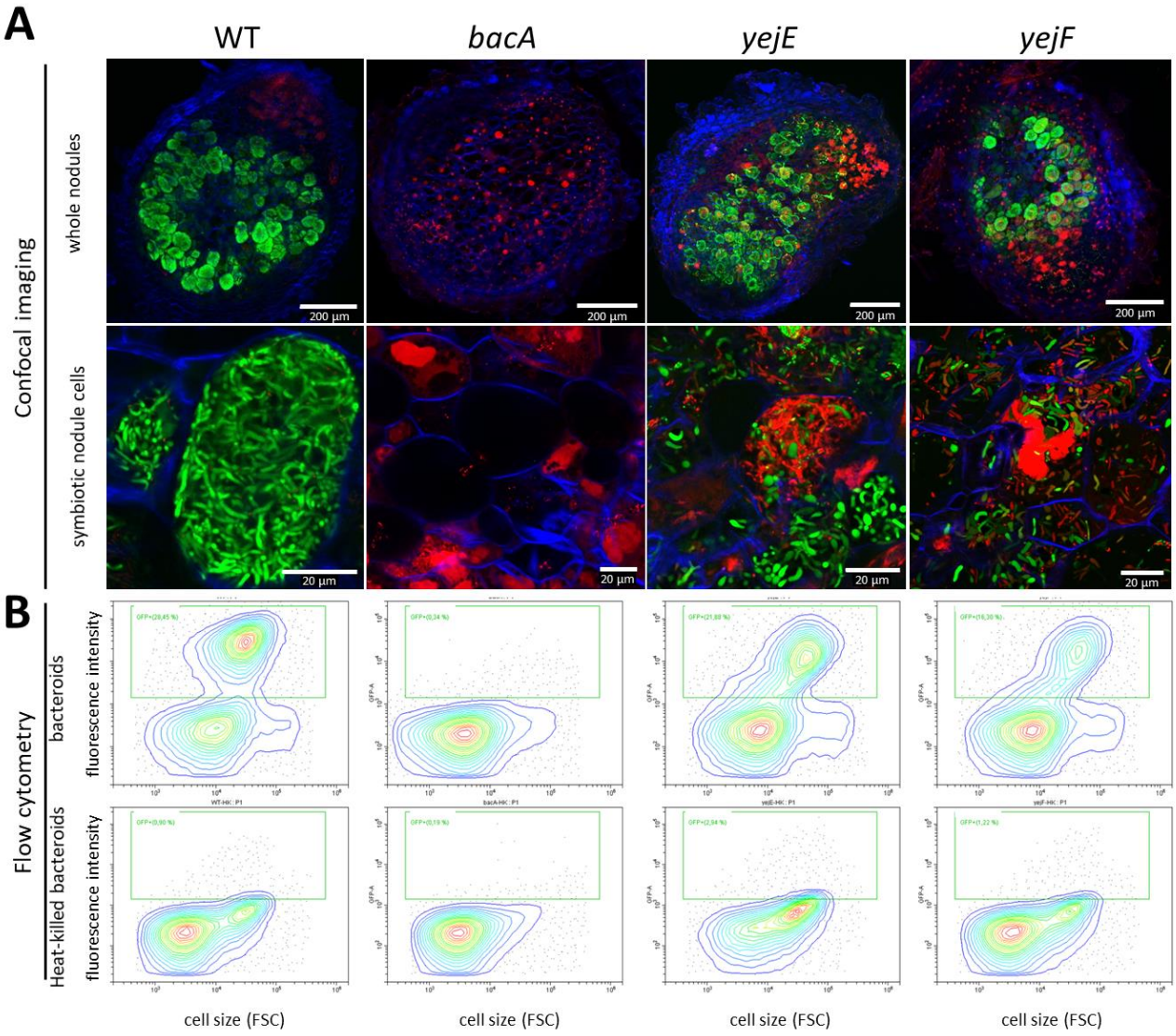
A
WT
bacA
yejE
yejF
Confocal imaging
whole nodules
symbiotic nodule cells
200 µm
20 µm
B
Flow cytometry
bacteroids
Heat-killed bacteroids
fluorescence intensity
cell size (FSC)

Figure 6

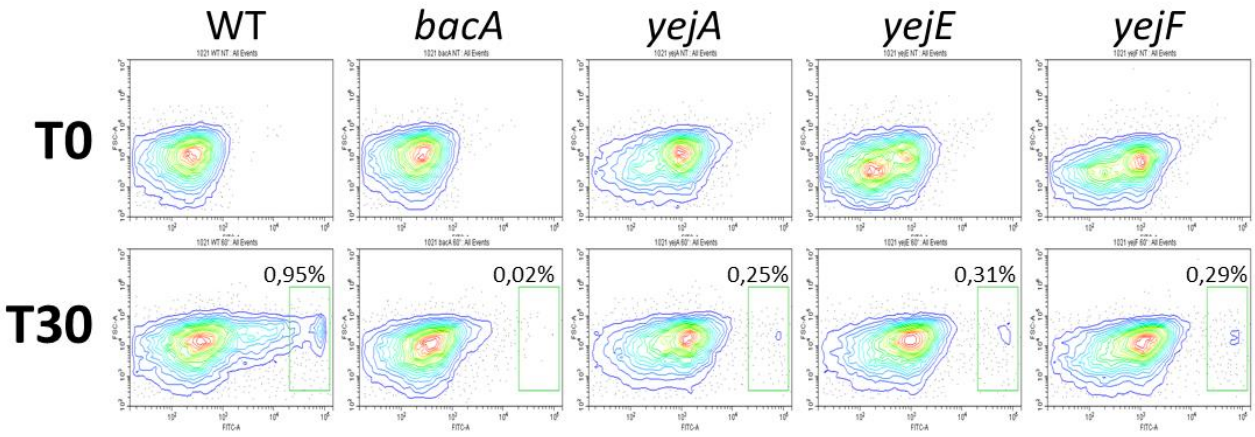

Figure S1

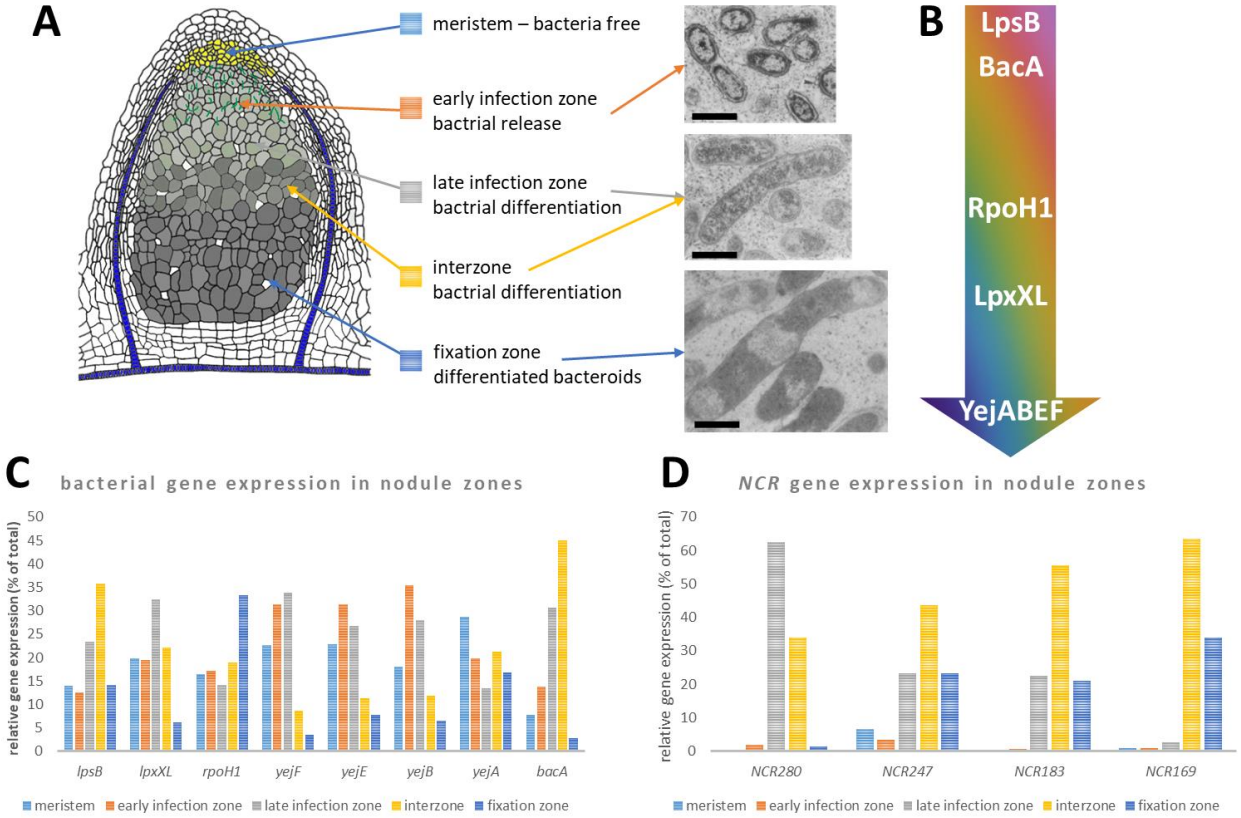
A
meristem – bacteria free
early infection zone
bactrial release
late infection zone
bactrial differentiation
interzone
bactrial differentiation
fixation zone
differentiated bacteroids
B
LpsB
BacA
RpoH1
LpxXL
YejABEF
C
bacterial gene expression in nodule zones
relative gene expression (% of total)
lpsB
lpxXL
rpoH1
yejF
yejE
yejB
yejA
bacA
meristem
early infection zone
late infection zone
interzone
fixation zone
D
NCR gene expression in nodule zones
relative gene expression (% of total)
NCR280
NCR247
NCR183
NCR169
meristem
early infection zone
late infection zone
interzone
fixation zone

Figure S2

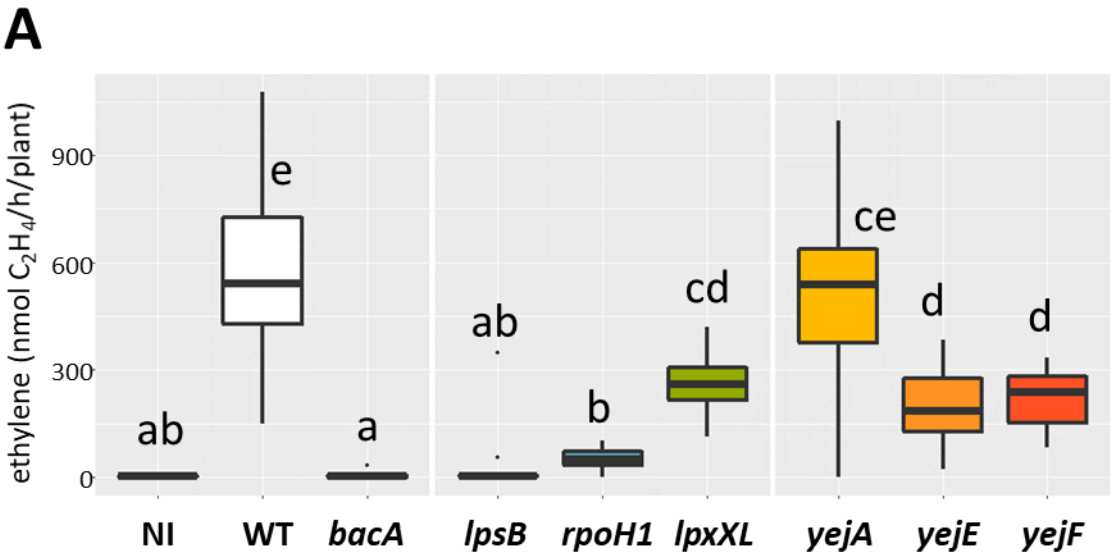
A
ethylene (nmol C_2H_4/h/plant)
900
600
300
0
ab
e
a
ab
b
cd
ce
d
d
NI
WT
bacA
lpsB
rpoH1
lpxXL
yejA
yejE
yejF

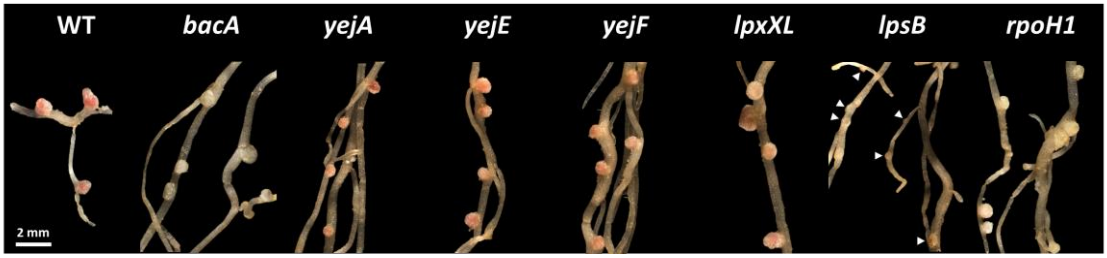
B
WT
bacA
yejA
yejE
yejF
lpxXL
lpsB
rpoH1
2 mm

Figure S3

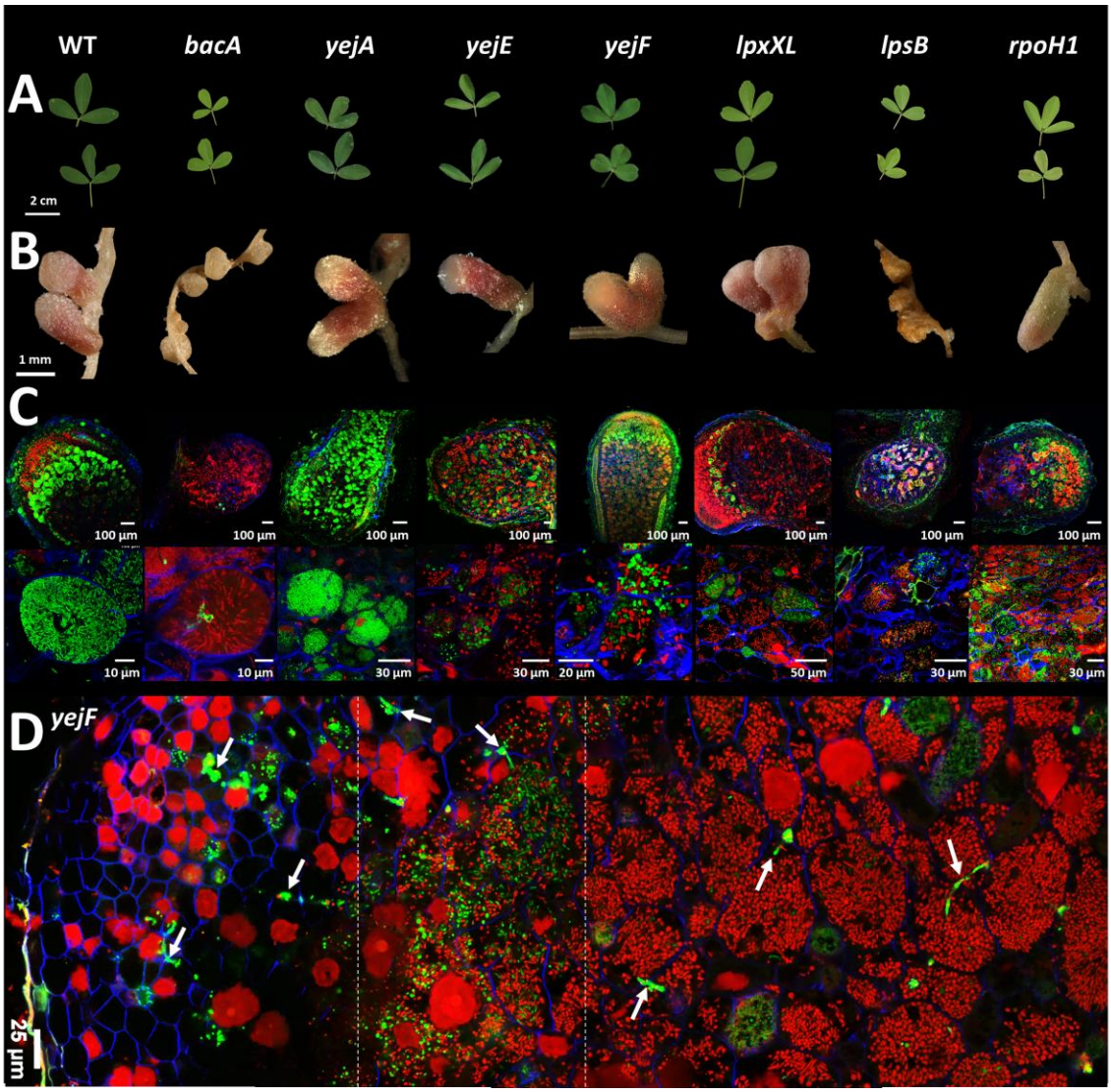
WT
bacA
yejA
yejE
yejF
lpxXL
lpsB
rpoH1
A
2 cm
B
1 mm
C
100 µm
10 µm
30 µm
20 µm
50 µm
D
yejF
25 µm

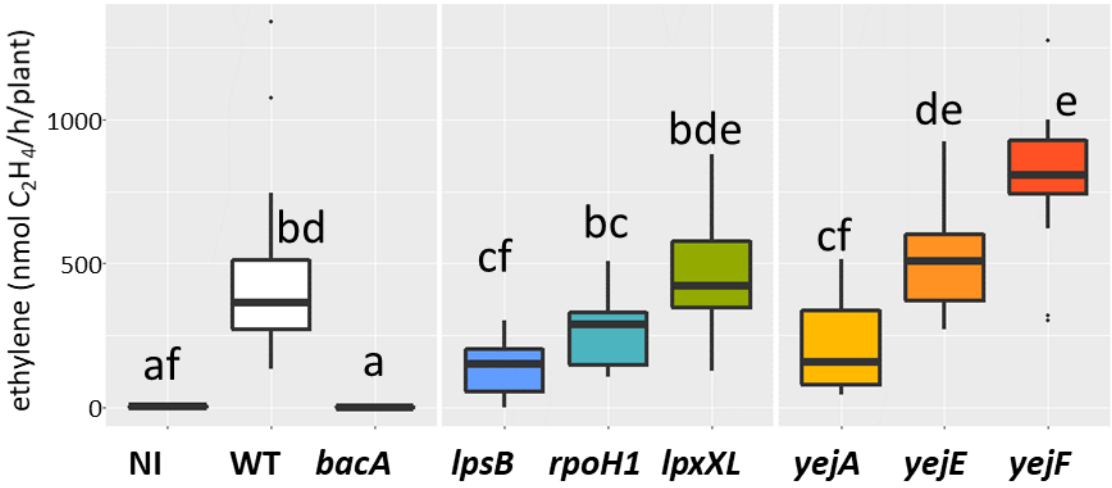
E
ethylene (nmol C_2H_4/h/plant)
1000
500
0
af
bd
a
cf
bc
bde
cf
de
e
NI
WT
bacA
lpsB
rpoH1
lpxXL
yejA
yejE
yejF

Figure S4

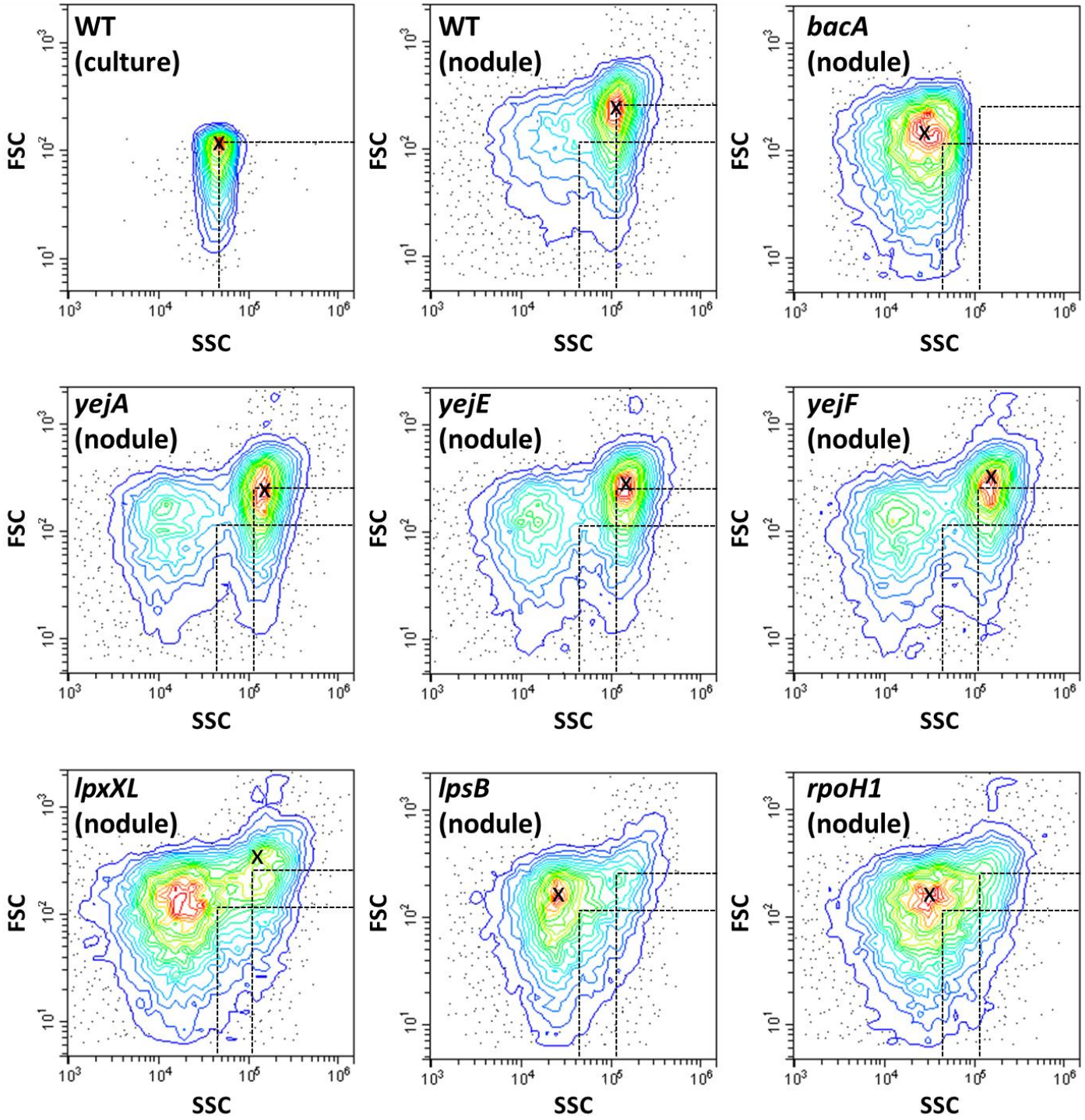
WT
(culture)
WT
(nodule)
bacA
(nodule)
yejA
(nodule)
yejE
(nodule)
yejF
(nodule)
lpxXL
(nodule)
lpsB
(nodule)
rpoH1
(nodule)
FSC
SSC
10^1
10^2
10^3
10^4
10^5
10^6

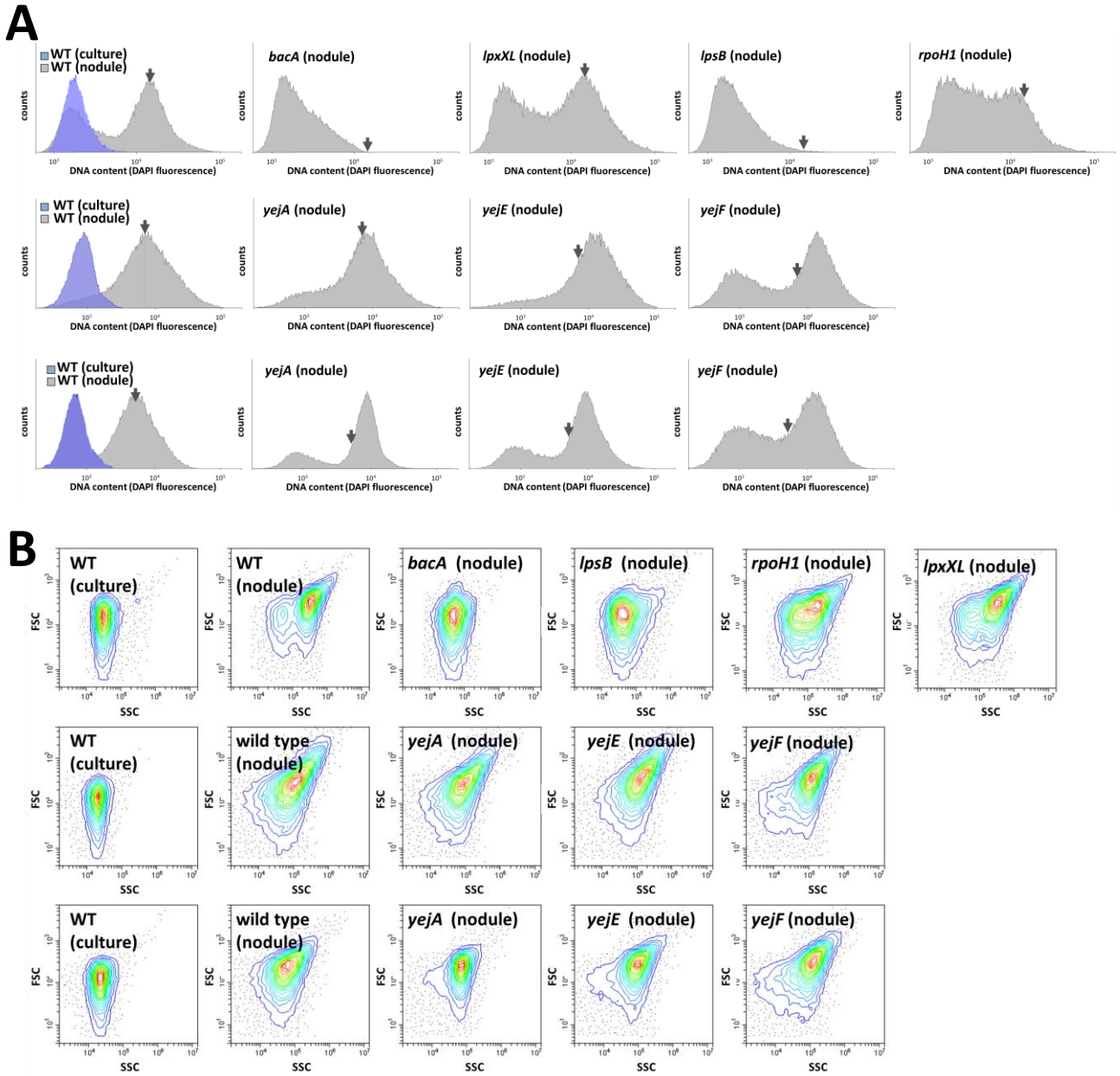
A
WT (culture)
WT (nodule)
bacA (nodule)
lpxXL (nodule)
lpsB (nodule)
rpoH1 (nodule)
yejA (nodule)
yejE (nodule)
yejF (nodule)
counts
DNA content (DAPI fluorescence)
B
WT (culture)
WT (nodule)
bacA (nodule)
lpsB (nodule)
rpoH1 (nodule)
lpxXL (nodule)
wild type (nodule)
yejA (nodule)
yejE (nodule)
yejF (nodule)
FSC
SSC

Figure S5

Figure S6

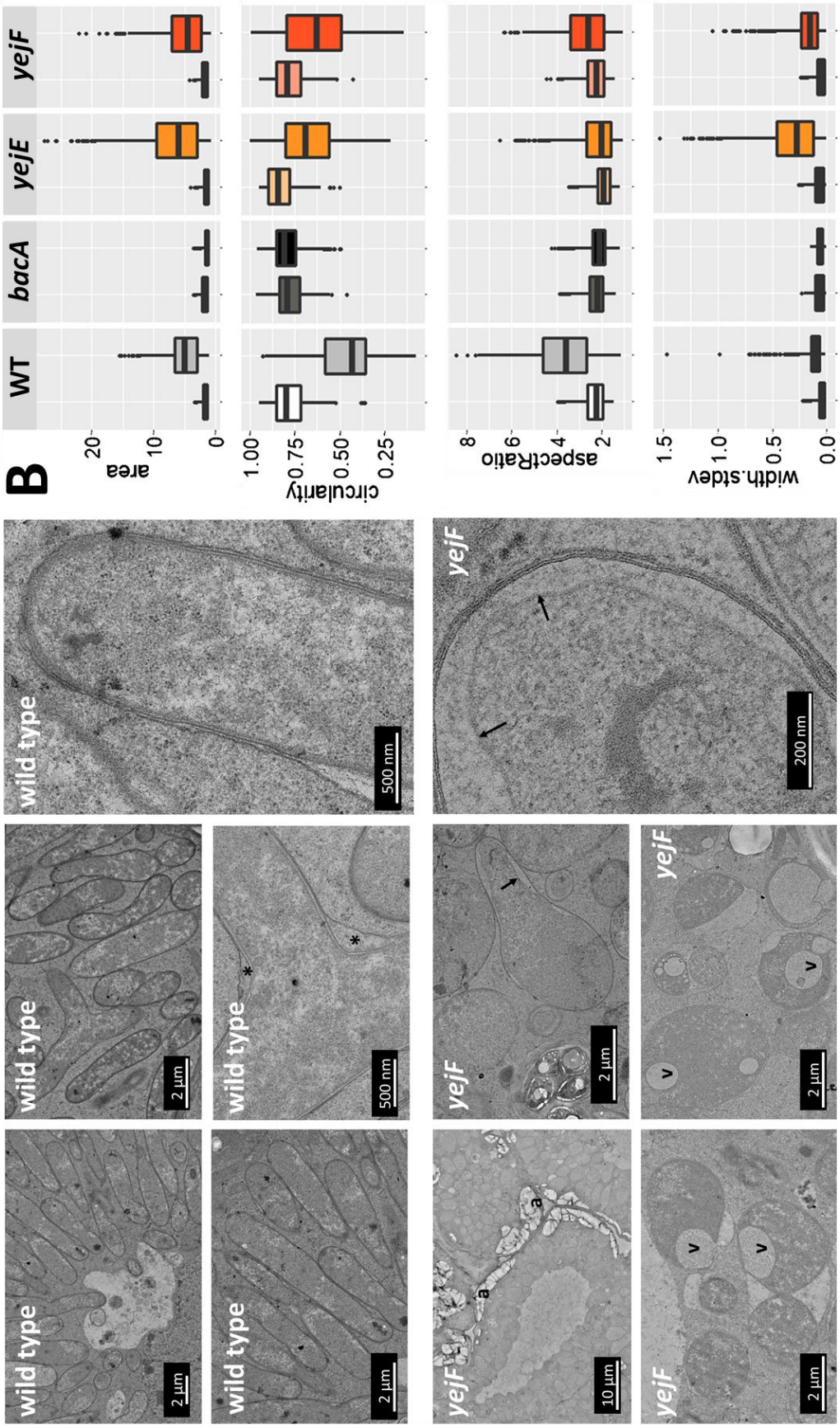
A
wild type
2 µm
wild type
2 µm
wild type
500 nm
wild type
500 nm
wild type
2 µm
wild type
500 nm
yejF
10 µm
a
a
yejF
2 µm
yejF
200 nm
yejF
2 µm
v
v
yejF
2 µm
v
v
B
WT
bacA
yejE
yejF
area
20
10
0
circularity
1.00
0.75
0.50
0.25
aspectRatio
8
6
4
2
width.stdev
1.5
1.0
0.5
0.0

Figure S7

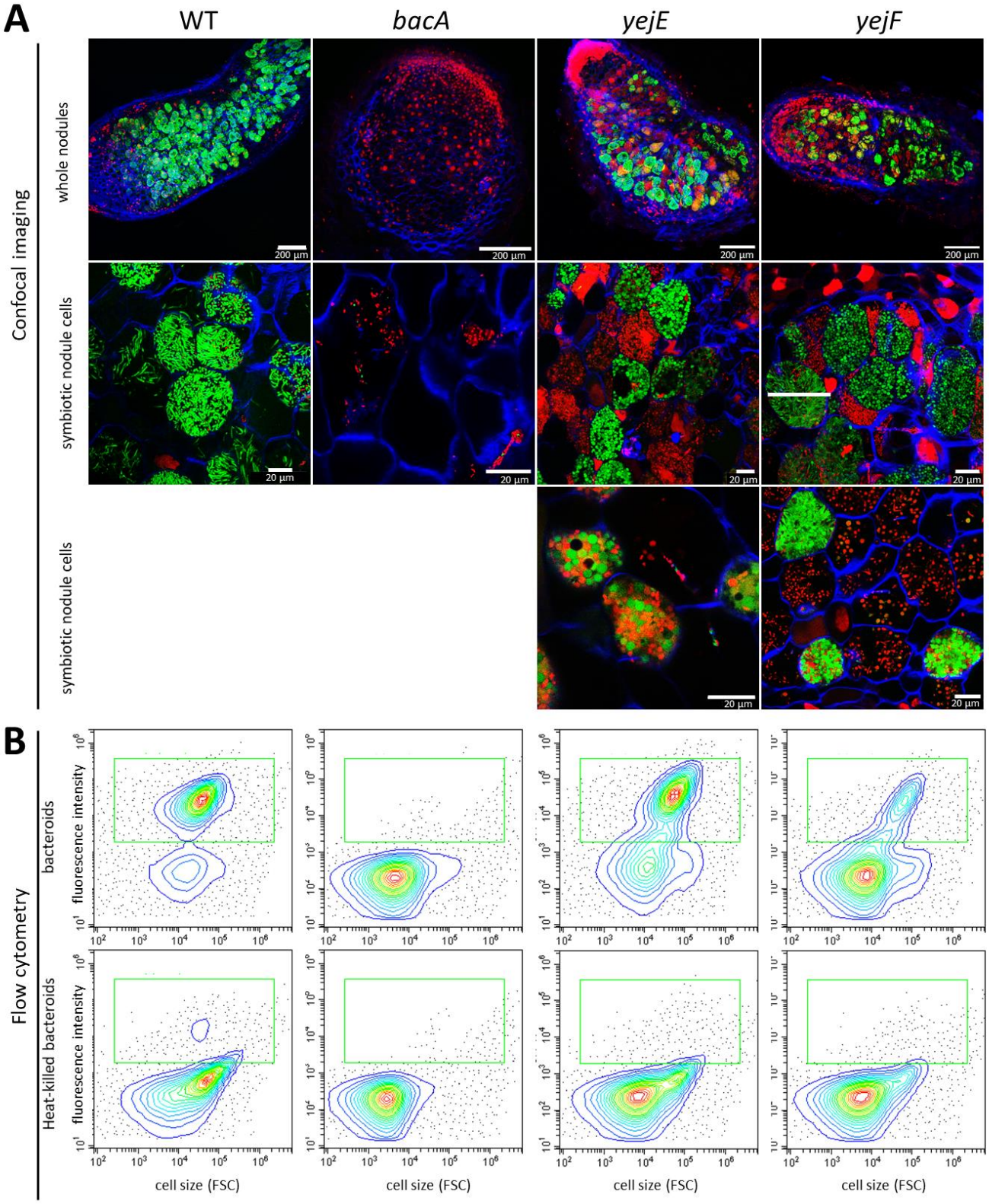
A
WT
bacA
yejE
yejF
Confocal imaging
whole nodules
symbiotic nodule cells
symbiotic nodule cells
200 µm
20 µm
B
Flow cytometry
bacteroids
Heat-killed bacteroids
fluorescence intensity
cell size (FSC)

Figure S8

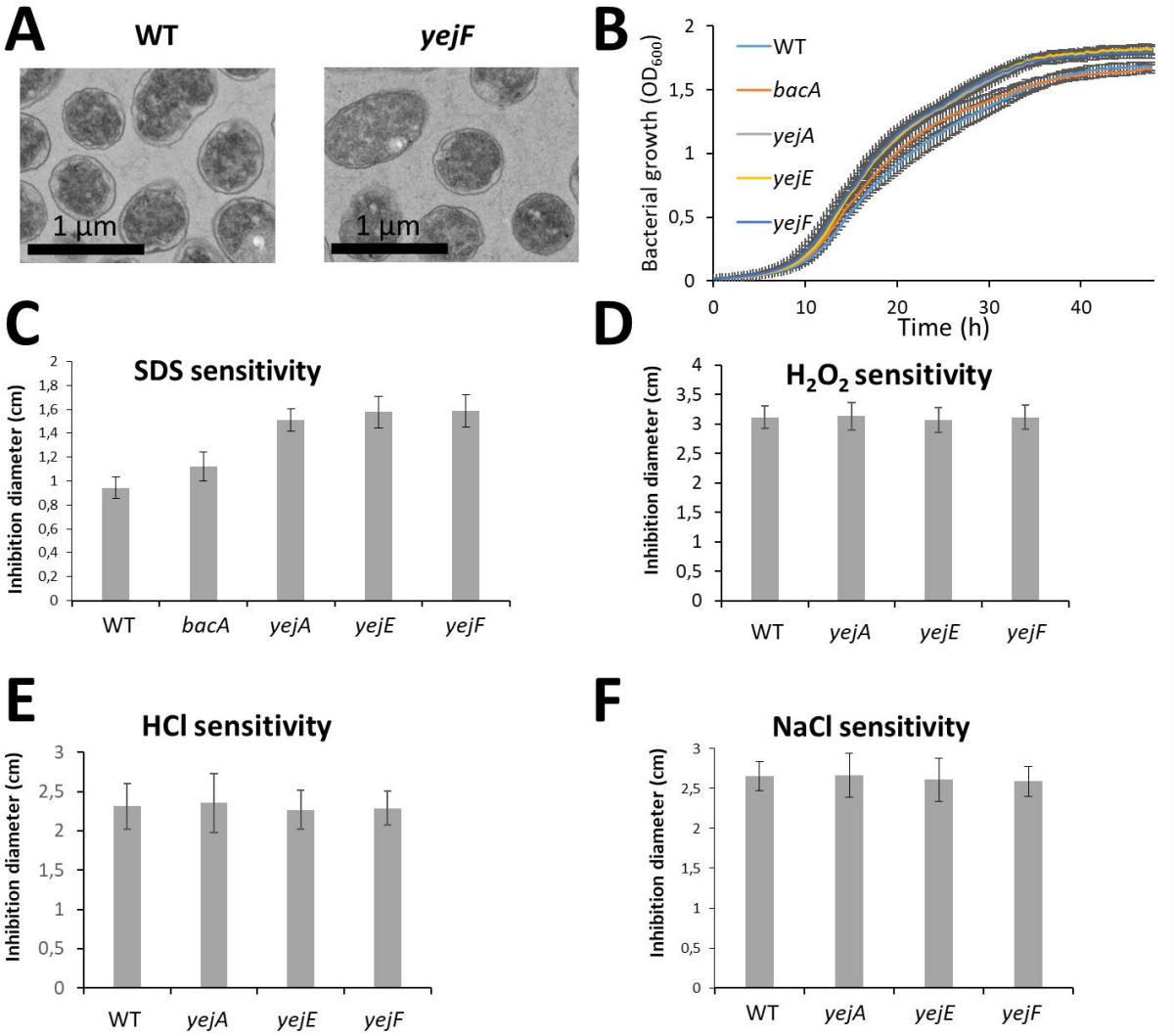
A
WT
yejF
1 µm
1 µm
B
Bacterial growth (OD600)
Time (h)
WT
bacA
yejA
yejE
yejF
C
SDS sensitivity
Inhibition diameter (cm)
WT
bacA
yejA
yejE
yejF
D
H2O2 sensitivity
Inhibition diameter (cm)
WT
yejA
yejE
yejF
E
HCl sensitivity
Inhibition diameter (cm)
WT
yejA
yejE
yejF
F
NaCl sensitivity
Inhibition diameter (cm)
WT
yejA
yejE
yejF

peptide (concentration)	survival (%) relative to untreated bacteria (n=3)	Standard deviation	survival relative to WT (%)
NCR169 (10 µM)			
WT	8,72727273	3,40708416	100
bacA	4,8	4,42920941	55
yejA	10,9090909	8,51771041	125
yejE	9,45454545	1,70354208	108,333333
yejF	13,6727273	8,85841882	156,666667
lpxXL	1,01818182	0,34070842	11,6666667
lpsB	6,54545455	1,70354208	75
rpoH	7,56363636	0,68141683	86,6666667
NCR183 (10 µM)			
WT	0,04654545	0,02725667	100
bacA	0,00581818	0,01362834	12,5
yejA	0,128	0,10902669	275
yejE	0	0	0
yejF	0	0	0
lpxXL	0	0	0
lpsB	0,00232727	0,00545133	5
rpoH	0,22690909	0,1499117	487,5
NCR247 (25 µM)			
WT	0,03025455	0,016354	100
bacA	0,00116364	0,00272567	3,84615385
yejA	0,04654545	0	153,846154
yejE	0,00116364	0,00272567	3,84615385
yejF	0	0	0
lpxXL	0	0	0
lpsB	0	0	0
rpoH	0	0	0
NCR280 (25 µM)			
WT	0,05352727	0,01090267	100
bacA	0,0128	0,02453101	23,9130435
yejA	0,00116364	0,00272567	2,17391304
yejE	0	0	0
yejF	0,00581818	0,01362834	10,8695652
lpxXL	0	0	0
lpsB	0	0	0
rpoH	*0,07214545*	*0,02180534*	*134,782609*

	Gene	Primer name	Sequence	Description
Insertion mutants	SMc02829 (*yejF*)	2829forward	CAAATCGGTGTCGACCAACTCGATCCTGAAGCTC	Primers used to amplify a region of *SMc02829* CDS, flanked with SalI & XbaI sites
		2829reverse	GTTGGCTCTAGACATGGCTATCATTAC	
		2829out-f	CATCTCCTTCGACATCAAG	Primers used for verification
		2829out-r	CTCGTCGGCGATCAGGAGCTC	
	SMc02830 (*yejE*)	2830forward	CTTCGGCCTGTCGACGTTTGCCGAGTTCATC	Primers used to amplify a region of *SMc02830* CDS, flanked with SalI & XbaI sites
		2830reverse	CAGCGCTCTAGAGAAAAGGACCGAGATG	
		2830out-f	CTGGCTCTTCCTCCTCCTCTTC	Primers used for verification
		2830out-r	GATGATGAGCAGGATGTAGAG	
	SMc02832 (*yejA*)	2832forward	GCTACGTCGACGATCGGAGAACCCAAATAC	Primers used to amplify a region of *SMc02832* CDS, flanked with SalI & XbaI sites
		2832reverse	GTGACTCTAGACTCGCCTGTCTTTTC	
		2832out-f	CAATGCCGAGGAACAACC	Primers used for verification
		2832out-r	GAGAATGTTCGGCAGTTC	
	SMc00646 (*rpoH1*)	RpoH1-Sal1-forward	CGCACAGTCGACTAACGAGCCATCTTCGCCTC	Primers used to amplify a region of *SMc00646* CDS, flanked with SalI & XbaI sites
		RpoH1-Xba1-Reverse	CGAAGATCTAGAGCTCACGATCGTTCAGAACC	
		RpoH1-up	AAGCGGTATCAGGAG	Primers used for verification
		RpoH1-down	CCTCCTGCACCTTTT	
Deletion mutants	SMc02829 (*yejF*)	2829fup	GCAACGGCACCATCATGGATCCGCACC	Up fragment used for deletion of *SMc02829*
		2829rup	GGAGAAACTCGGAACGTCTTTCTCG	
		2829fdown	CGTTCCGAGTTTCTCCCATGC	Down fragment used for deletion of *SMc02829*
		2829rdown	CACCCACTCGCTCATCCAAGCTTTCAGG	
	SMc02830 (*yejE*)	2830fup	GGACACGTGTTCCGCAACGGATCCCTGATC	Up fragment used for deletion of *SMc02830*
		2830rup	CGTCGCGCCAGACGTCCCTCCG	
		2830fdown	GGACGTCTGGCGCGACGATGACAG	Down fragment used for deletion of *SMc02830*
		2830rdown	GCGAACATGCCTGAAAGCTTCGTCG	
	SMc02832 (*yejA*)	2832fup	GGTCGAACCGCAGGGATCCAGCGCAGCACG	Up fragment used for deletion of *SMc02832*
		2832rup	GCAAGAGCTCCGGCCGGTACCCC	
		2832fdown	CGGCCGGAGCTCTTGCGCTCAGG	Down fragment used for deletion of *SMc02832*
		2832rdown	CATGATGCCGACGATCGTCAAGCTTATCAGC	